Rayleigh-Taylor and Richtmyer-Meshkov instabilities and mixing in stratified spherical shells

Karnig O. Mikaelian
Lawrence Livermore National Laboratory, Livermore, California 94550
(Received 29 September 1989; revised manuscript received 22 January 1990)

We study the linear stability of an arbitrary number of spherical concentric shells undergoing a radial implosion or explosion. The system consists of N incompressible fluids with small amplitude perturbations at each of the $N-1$ interfaces. We derive the evolution equation for the perturbation η_i at interface i; it is coupled to the two adjacent interfaces via $\eta_{i\pm1}$. We show that the $N-1$ evolution equations are symmetric under $n \Longleftrightarrow -n-1$, where n is the mode number of the spherical perturbation, provided that the first and last fluids have zero density ($\rho_1=\rho_N=0$). In plane geometry this translates to symmetry under $k \Longleftrightarrow -k$. We obtain several analytic solutions for the $N=2$ and 3 cases that we consider in some detail. As an application we derive the shock timing that is required to freeze out an amplitude. We also identify "critical modes" that are stable for any implosion or explosion history. Several numerical examples are presented illustrating perturbation feedthrough from one interface to another. Finally, we develop a model for the evolution of turbulent mix in spherical geometry, and introduce a geometrical factor G relating the mixing width h in spherical and planar geometries via $h_{\text{spherical}}=h_{\text{planar}}G$. We find that G is a decreasing function of R/R_0, implying that in our model $h_{\text{spherical}}$ evolves faster (slower) than h_{planar} during an implosion (explosion).

I. INTRODUCTION AND NOTATION

The classical Rayleigh-Taylor instability[1] refers to the evolution of perturbations at the interface between two fluids undergoing a constant acceleration. The Richtmyer-Meshkov instability[2] occurs when the interface is subjected to a shock. Most of the theoretical, computational, and experimental work has been in plane geometry and two fluids only.[3] A few years ago we extended the Rayleigh-Taylor problem to an arbitrary number of fluids,[4] and similarly for the Richtmyer-Meshkov problem.[5] The purpose of this paper is to carry out a similar extension to multilayer fluids in spherical geometry. We believe that a recent paper[6] claiming to have done just such an extension is incorrect.

We mention two applications in which spherical geometry may be important: one is the implosion of inertial confinement fusion (ICF) capsules, in which we are primarily interested. The second is stellar collapse when, for example, a shock helps eject most of the material in a supernova explosion. We expect that the Rayleigh-Taylor and Richtmyer-Meshkov instabilities lead to mixing in ICF capsules or stars as the interfaces between two different materials are subjected to accelerations or shocks. Due to the complexity and nonlinear nature of turbulent mixing we will conclude this paper by presenting a model, in the form of an *ansatz*, to estimate the mixing widths in spherical geometry. Otherwise the bulk of this paper treats the linear regime much the way it was done in plane geometry, i.e., we assume that perturbations are small, that the fluids are incompressible, and we neglect viscosity, surface tension, and heat conduction. These are the usual classical assumptions which allow the analysis to proceed from basic principles.

We now review briefly earlier work in spherical geometry. The first application was apparently the stability of a spherical cavity. Perturbations at the interface between the cavity and the outer fluid are expanded in spherical harmonics $Y_{n,m}$. The amplitude η of the nth mode evolves according to[7]

$$\frac{d^2\eta}{dt^2}+3\frac{\dot R}{R}\frac{d\eta}{dt}-(n-1)\frac{\ddot R}{R}\eta=0 \tag{1}$$

and the conditions for stability were given by Birkhoff.[8] Binnie[9] considered the case where the central cavity is replaced by a fluid of density ρ_1. His results were in error and subsequently Plesset[10] produced the correct evolution equation for this case:

$$\frac{d^2\eta}{dt^2}+3\frac{\dot R}{R}\frac{d\eta}{dt}-nA(n)\frac{\ddot R}{R}\eta=0\ , \tag{2}$$

where

$$nA(n)=\frac{n(n-1)\rho_2-(n+1)(n+2)\rho_1}{n\rho_2+(n+1)\rho_1}\ , \tag{3}$$

ρ_2 being the density of the outer fluid. He also pointed out that an incompressible fluid of finite density ρ_1 implies a source or a sink at the origin. As expected, Eq. (2) reduces to Eq. (1) for the case of a spherical cavity ($\rho_1=0$). We will refer to Eq. (2) as "Plesset's equation." Its stability conditions were also given by Birkhoff:[8]

$$nA(n)\ddot R<0,\quad \frac{d}{dt}[nA(n)R^5\ddot R]<0\ . \tag{4}$$

Considering the same problem Gupta and Lawande[11] assumed a constant radial acceleration and perturbations

growing exponentially in time, as was done by Binnie. The results of Gupta and Lawande and of Binnie, which are identical, do not reduce to the spherical cavity case when $\rho_1=0$. We have already presented our comments and comparisons on this two-fluid problem.[12]

In treating the general problem of N spherical fluid layers Gupta and Lawande[6] continued to assume a constant acceleration and exponentially growing perturbations. For $N=2$ one may assume a constant g and in fact we consider it as a special case later in this paper (but we find that the perturbations do not grow exponentially in time). For $N>2$, however, one cannot assume a constant acceleration at all interfaces. Conservation of mass or volume (the two are equivalent because we are considering incompressible fluids) allows one to specify the motion of *only* one interface—say, $R_i(t)$. The motion of all the other interfaces $R_j(t)$ is then fixed by volume conservation

$$R_j(t)=[R_j^3(0)-R_i^3(0)+R_i^3(t)]^{1/3}$$

and clearly if the acceleration is constant at one interface it *cannot* be constant at any other interface. This is a purely geometric requirement (exactly the opposite is true in plane geometry: mass conservation of incompressible planar fluid layers requires that the acceleration be the same at all interfaces). This obvious shortcoming of the work of Gupta and Lawande[6] was the primary motive for carrying out the research reported here.

Our notation is defined in Fig. 1: it shows a spherical fluid of density ρ_1 and radius R_1 surrounded by a series of concentric shells. There are N fluids of densities $\rho_1,\rho_2,\ldots,\rho_N$. The interface between shells i and $i+1$, of densities ρ_i and ρ_{i+1}, has a radius $R_i(t)$. The last fluid, of density ρ_N, is assumed to have $R_N=\infty$, hence there are $N-1$ finite radii $R_1,R_2,\ldots,R_{N-1}$. We denote radial velocities and accelerations by $v_i(t)$ and $g_i(t)$,

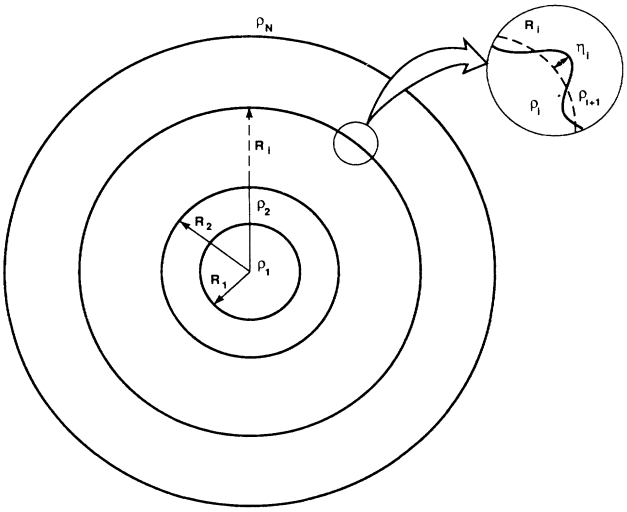

FIG. 1. N-fluid system in spherical geometry considered in this paper. The successive densities are $\rho_1,\rho_2,\ldots,\rho_{N-1},\rho_N$, and the radii are $R_1,R_2,\ldots,R_{N-1}$. R_i is the average radius of the interface between the two fluids of densities ρ_i and ρ_{i+1}, and has a perturbation of amplitude η_i.

$$\frac{dR_i(t)}{dt}=\dot{R}_i(t)=v_i(t),\quad \frac{d^2R_i(t)}{dt^2}=\ddot{R}_i(t)=g_i(t)\ ,$$

and drop the labeling subscript i when no confusion can arise. Initial values will be denoted also by a zero subscript as in $R(0)=R_0$ or $\eta(0)=\eta_0$. Positions within a fluid layer will be denoted by r. Perturbations are introduced by a straightforward generalization of Plesset's treatment: each interface is assumed to have a perturbation of mode (n,m) so that

$$r_i(t)=R_i(t)+\eta_i(t,n,m)Y_{n,m}(\theta,\varphi)\ , \tag{5}$$

with

$$|\eta_i(t,n,m)|\ll R_i(t) \tag{6}$$

at each interface.

Two remarks are in order: first, condition (6) above is not enough for the linear analysis; one also needs

$$|n\eta_i(t,n,m)|\ll R_i(t) \tag{7}$$

as we will show in Sec. II. While Plesset explicitly mentions only condition (6), he implicitly uses the much more restrictive condition (7). Second, Plesset's single amplitude analysis applies also to each mode in an arbitrary perturbation as long as they all remain in the linear regime. This was pointed out by Plesset and Mitchell[13] and follows trivially from the orthogonality of the spherical harmonics.

We close this section by recalling well-known classical results in a planar geometry for $N=2$. For a constant acceleration,[1]

$$\eta=\eta_0\cosh(\gamma t)+\frac{\dot{\eta}_0}{\gamma}\sinh(\gamma t)\ , \tag{8}$$

where the growth rate $\gamma=\sqrt{gkA}$, $k=2\pi/\lambda$, and λ represents the wavelength of the perturbation, and A represents the Atwood number

$$A=\frac{\rho_2-\rho_1}{\rho_2+\rho_1}\ . \tag{9}$$

For a shock treated as an impulsive acceleration, $g=\Delta v\,\delta(t)$, we get

$$\dot{\eta}(0_+)=\dot{\eta}(0_-)+kA\Delta v\,\eta(0)\ , \tag{10}$$

where the subscripts $\pm$ refer to postshock (preshock) values. In this incompressible treatment, suggested by Richtmyer,[2] the shock changes the growth rate $\dot{\eta}$ of the perturbations without changing η instantaneously, i.e., $\eta(0_+)=\eta(0_-)=\eta(0)$. The subsequent evolution of η depends on the motion of the fluids—if it is a constant acceleration, for example, then η is given by Eq. (8) with $\dot{\eta}(0)=\dot{\eta}(0_+)$.

We chose our notation with an eye towards an easy transition to the planar limit, which is done by taking $n\to\infty$, $R\to\infty$, with $k=n/R$ finite. The coefficient $A(n)$ in Plesset's equation was chosen such that

$$A(n)\to A \quad \text{as } n\to\infty$$

and the equation reduces to the well-known result

$$\frac{d^2\eta}{dt^2}-gkA\eta=0$$

in the planar limit.

The condition for linearity is $k\eta \ll 1$ in plane geometry and it is our more restrictive requirement, Eq. (7), which reduces to it.

In Sec. II we derive the general equation governing the evolution of the perturbation η_i at each interface. As in the planar case, we find that η_i is coupled to the two adjacent surface perturbations $\eta_{i\pm1}$, and in this way all perturbations are coupled to each other through the intermediate ones. In Sec. III we specialize to $N=2$ where our equations reduce to Plesset's equation, and we consider several cases where analytic solutions can be written down explicitly. Particular emphasis is given to shocks, leaving mathematical details and other solutions to the Appendix. In Sec. IV we study the $N=3$ case; unlike the planar case where the solution for arbitrary densities and thicknesses could be written down in a fairly simple form, in spherical geometry the coupled equations are quite complex and require a numerical solution which we present for an imploding and an exploding system. We also present analytic expressions for the special case $\rho_1=\rho_3=0$ and in the limit where the thickness of the intermediate shell is much less than its radius. In Sec. V we present a model for calculating the turbulent mixing width h in spherical geometry. Finally, in Sec. VI we present our concluding remarks and possible directions for future work.

II. GENERAL EVOLUTION EQUATIONS

Referring to Fig. 1, we introduce a velocity potential φ_i in each region i of density ρ_i extending between r_{i-1} and r_i such that the fluid velocity in that region is given by $-\partial\varphi_i/\partial r$. Since we assume incompressible flow, $\nabla^2\varphi_i=0$, hence φ_i is given in terms of the solution to Laplace's equation in spherical geometry. As in Ref. 10, we require that the perturbation velocities vanish at the center and at infinity, hence $\varphi_1\sim r^n$ and $\varphi_N\sim r^{-n-1}$ in the first and last zones, respectively. In the intermediate layers, however, one must consider a linear superposition of the two forms:[14]

$$\varphi_i=\frac{R_i^2\dot{R}_i}{r}+B_i r^n Y_{n,m}+C_i Y_{n,m}/r^{n+1}\ , \tag{11}$$

where B_i and C_i are constants to be determined via continuity of the radial velocity. They are functions of n, m, R_i, R_{i-1}, etc. and are constants only in the sense that they do not vary with position within each shell, i.e., $B_i,C_i\neq B_i(r),C_i(r)$. Therefore

$$-\left.\frac{\partial\varphi_i}{\partial r}\right|_{r_i}=\frac{R_i^2\dot{R}_i}{r_i^2}-nB_i r_i^{n-1}Y_{n,m}+(n+1)C_i Y_{n,m}/r_i^{n+2}\ , \tag{12a}$$

$$-\left.\frac{\partial\varphi_i}{\partial r}\right|_{r_i}=\dot{r}_i=\dot{R}_i+\dot{\eta}_i Y_{n,m}\ , \tag{12b}$$

where the second equation follows from Eq. (5). Since the velocity potential φ_i in Eq. (11) holds in the region $r_{i-1}\le r\le r_i$, we obtain two more equations identical to (12a) and (12b) with r_i replaced by r_{i-1}. Equating the right-hand sides of Eqs. (12a) and (12b), and the corresponding ones with $r_i\to r_{i-1}$, we will obtain two equations which determine the two constants B_i and C_i explicitly if we limit ourselves to the linear regime. The reason for the linear approximation is that we need to substitute $r_i=R_i+\eta_i Y_{n,m}$ in Eq. (12a) and without the assumption of linearity the expressions become quite complicated.

In the absence of any perturbations B_i and C_i in Eq. (11) vanish and, therefore, they are at least of order η. In the first term of Eq. (12a) we approximate $r_i^{-2}=(R_i+\eta_i Y_{n,m})^{-2}\approx R_i^{-2}(1-2\eta_i Y_{n,m}/R_i)$ which requires only the weak linearity condition Eq. (6). The second and third terms of Eq. (12a) are proportional to B_i and C_i which are already of order η_i. We will therefore use the lowest-order relation ($r_i\to R_i$) in expanding r_i^{n-1} and r_i^{-n-2}, i.e., replace them by R_i^{n-1} and R_i^{-n-2}, respectively. For this to be a valid procedure we obviously require the stronger linearity condition Eq. (7).

As expected, the zeroth-order ($\dot{R}_i$) terms on the right-hand side (rhs) of Eq. (12a) and (12b) cancel, leaving a result that is linear in η_i and its first time derivative $\dot{\eta}_i$:

$$nB_i=\left[(n+1)C_iR_i^{-n-2}-2\frac{\dot{R}_i}{R_i}\eta_i-\dot{\eta}_i\right]\Big/R_i^{n-1}\ . \tag{13a}$$

We now repeat the same procedure at interface $i-1$. Since B_i and C_i are *regional* quantities, they remain the same. The result is

$$nB_i=\frac{\left[(n+1)C_i(R_{i-1})^{-n-2}-2\dfrac{\dot{R}_{i-1}}{R_{i-1}}\eta_{i-1}-\dot{\eta}_{i-1}\right]}{(R_{i-1})^{n-1}}\ . \tag{13b}$$

Note that the zeroth-order terms ($\dot{R}_{i-1}$) have again canceled because $R_i^2\dot{R}_i=(R_{i-1})^2\dot{R}_{i-1}$, i.e., the quantity $R^2\dot{R}$ is the same at *all* interfaces, which is simply a consequence of mass (or volume) conservation: $R_j^3-R_i^3=$const in time. Mass conservation is not required for the two-fluid case where there is only one interface and hence only one equation.

Equations (13a) and (13b) determine the two constants B_i and C_i. After some algebra we get

$$B_i=\frac{-(R_i)^{-n-1}}{n[1-(R_{i-1}/R_i)^{2n+1}]}\frac{d}{dt}(R_i^2\eta_i)+(i\Longleftrightarrow i-1)\ , \tag{14}$$

$$C_i=B_i(n\to -n-1)\ , \tag{15}$$

which completely specify the velocity potential φ_i in Eq. (11).

To get the equations of motion for the interface radii $R_i(t)$ and the evolution equations for the perturbations $\eta_i(t)$ we follow Plesset's method but leave out surface

tension for simplicity. In this case the pressure on each side of the interface at r_i is continuous and therefore

$$P_i(t)+\rho_i\left[\frac{\partial\varphi_i}{\partial t}-\tfrac{1}{2}(\nabla\varphi_i)^2\right]_{r_i} =P_{i+1}(t)+\rho_{i+1}\left[\frac{\partial\varphi_{i+1}}{\partial t}-\tfrac{1}{2}(\nabla\varphi_{i+1})^2\right]_{r_i}, \tag{16}$$

where $P_{i,i+1}(t)$ are the constants of the spatial integration leading to the Bernoulli integral. To lowest order in η_i

$$\left.\frac{\partial\varphi_i}{\partial t}\right|_{r_i=R_i+\eta_i Y_{n,m}} =\frac{1}{R_i}\left[1-\frac{\eta_i}{R_i}Y_{n,m}\right]\frac{d}{dt}(R_i^2\dot R_i) +R_i^n Y_{n,m}\frac{dB_i}{dt}+\frac{Y_{n,m}}{R_i^{n+1}}\frac{dC_i}{dt}, \tag{17a}$$

where we have again used the fact that B_i and C_i are already of order η_i so that we need to keep only the lowest-order term ($r_i\to R_i$) in their coefficients. Similarly, we evaluate

$$\left.\frac{\partial\varphi_{i+1}}{\partial t}\right|_{r_i=R_i+\eta_i Y_{n,m}} =\frac{1}{R_i}\left[1-\frac{\eta_i}{R_i}Y_{n,m}\right]\frac{d}{dt}(R_i^2\dot R_i) +R_i^n Y_{n,m}\frac{dB_{i+1}}{dt}+\frac{Y_{n,m}}{R_i^{n+1}}\frac{dC_{i+1}}{dt} \tag{17b}$$

again using mass conservation to set $(R_{i+1})^2\dot R_{i+1}=R_i^2\dot R_i$. Substituting Eqs. (17a) and (17b) in Eq. (16) and using the first-order approximation $(\nabla\varphi_i)^2|_{r_i}\approx(\nabla\varphi_{i+1})^2|_{r_i}\approx\dot r_i^2 \approx\dot R_i^2+2\dot\eta_i\dot R_i Y_{n,m}$, Eq. (16) reduces to

$$P_i+\rho_i\left[\frac{1}{R_i}\frac{d}{dt}(R_i^2\dot R_i)-\frac{\eta_i}{R_i^2}Y_{n,m}\frac{d}{dt}(R_i^2\dot R_i)+R_i^n Y_{n,m}\frac{dB_i}{dt}+\frac{Y_{n,m}}{R_i^{n+1}}\frac{dC_i}{dt}-\frac{\dot R_i^2}{2}-\dot R_i\dot\eta_i Y_{n,m}\right] =P_{i+1}+\rho_{i+1}\left[\frac{1}{R_i}\frac{d}{dt}(R_i^2\dot R_i)-\frac{\eta_i}{R_i^2}Y_{n,m}\frac{d}{dt}(R_i^2\dot R_i)+R_i^n Y_{n,m}\frac{dB_{i+1}}{dt}+\frac{Y_{n,m}}{R_i^{n+1}}\frac{dC_{i+1}}{dt}-\frac{\dot R_i^2}{2}-\dot R_i\dot\eta_i Y_{n,m}\right]. \tag{18}$$

The zeroth-order terms that are independent of η_i lead to the equation of motion of the ith interface:

$$P_i-P_{i+1}=(\rho_{i+1}-\rho_i)\left[R_i\frac{d^2R_i}{dt^2}+\frac{3}{2}\dot R_i^2\right]. \tag{19}$$

The rest of the terms are linear in η_i or $\eta_{i\pm1}$ and their time derivatives, each multiplied by $Y_{n,m}$. Dropping the common factor $Y_{n,m}$ we get, after some algebra,

$$(\rho_{i+1}-\rho_i)\frac{d}{dt}(R_i^2\dot R_i\eta_i)=R_i^{n+2}\left[\rho_{i+1}\frac{dB_{i+1}}{dt}-\rho_i\frac{dB_i}{dt}\right] +(n\to-n-1). \tag{20}$$

This is the general evolution equation we were seeking. It describes the time evolution of the perturbation amplitude η_i at interface i in terms of $\eta_{i\pm1}$ and their time derivatives. It is a second-order differential equation because [see Eq. (14)] dB_i/dt involves $\eta_i,\dot\eta_i,\ddot\eta_i$ and also $\eta_{i-1},\dot\eta_{i-1},\ddot\eta_{i-1}$. We can write Eq. (20) in the following form:

$$\sum_{j=i-1}^{i+1}\left[a^j\frac{d^2}{dt^2}+b^j\frac{d}{dt}+c^j\right]\eta_j=0, \tag{21}$$

in which each of the nine coefficients a^j,b^j,c^j, $j=i-1,i,i+1$ is a function of the two adjacent densities ρ_i and ρ_{i+1}, the radii R_{i-1}, R_i, and R_{i+1}, their time derivatives and, of course, mode number n. There are $N-1$ equations in all because there are $N-1$ interfaces, i.e., $i=1,2,\ldots,N-1$. The first and last regions must be treated carefully because they extend over $0\le r\le R_1$ and $R_{N-1}\le r\le\infty$, respectively. As mentioned earlier, we must require that $C_1=B_N=0$. For ease of reference we will write out the first and last evolution equations explicitly:

$$(\rho_2-\rho_1)\frac{d}{dt}(R_1^2\dot R_1\eta_1)=R_1^{n+2}\rho_2\frac{dB_2}{dt}+(n\to-n-1) -R_1^{n+2}\rho_1\frac{dB_1}{dt}, \tag{22a}$$

$$(\rho_N-\rho_{N-1})\frac{d}{dt}[(R_{N-1})^2\dot R_{N-1}\eta_{N-1}] =-\rho_{N-1}\left[(R_{N-1})^{n+2}\frac{dB_{N-1}}{dt}+(n\to-n-1)\right] +\rho_N(R_{N-1})^{-n+1}\frac{dC_N}{dt}, \tag{22b}$$

where

$$B_1=-\frac{1}{nR_1^{n+1}}\frac{d}{dt}(R_1^2\eta_1), \tag{23a}$$

$$C_N=\frac{(R_{N-1})^n}{n+1}\frac{d}{dt}[(R_{N-1})^2\eta_{N-1}]. \tag{23b}$$

The evolution equations for the intermediate interfaces $i=2,3,\ldots,N-2$ cover no singular points so that Eq. (20) is well defined.

Let us make a few general remarks concerning the evolution equations. There is no hidden dependence on the densities—all the dependence on ρ_i is shown explicitly in Eq. (20) because the B_i are independent of ρ_i [see Eqs.

(14) and (15)]. Clearly, we need to specify only density *ratios* rather that absolute densities. Furthermore, since the fluids are assumed to be incompressible, all ρ_i are constants in time, but otherwise are not constrained. Had the factor R_i^{n+2} in Eq. (20) not been there, we could have integrated that equation with respect to time and thus reduced all of our $N-1$ second-order differential equations into first-order ones, a major feat. Unfortunately, the presence of the R_i^{n+2} factor spoils such luck. The only exception is a shock treated as an instantaneous acceleration, an approach first used by Richtmyer[2] for the two-fluid case in plane geometry. In such an approach the radii R_i as well as the amplitudes η_i remain unchanged, while their time derivatives change. By setting $\ddot{R}_i=\Delta v_i\delta(t)=[\dot{R}_i(0_+)-\dot{R}_i(0_-)]\delta(t)$ we integrate Eq. (20) for $0_-<t<0_+$ and obtain

$$(\rho_{i+1}-\rho_i)R_i^2\eta_i[\dot{R}_i(0_+)-\dot{R}_i(0_-)] =R_i^{n+2}[\rho_{i+1}\Delta B_{i+1}-\rho_i\Delta B_i]+(n\rightarrow -n-1)\ , \quad (24)$$

where $\Delta B_i=B_i(0_+)-B_i(0_-)$. This is an equation which relates postshock derivatives to their preshock values. Of course the interface coupling aspect remains the same, that is, Eq. (24) still involves the triad $\eta_{i-1},\eta_i,\eta_{i+1}$ and their first-order preshock and postshock derivatives.

Our next remark concerns the symmetry of Eq. (20). Clearly, Eq. (20) is invariant under

$$n\Longleftrightarrow -n-1 \quad (25)$$

and hence one might conclude that the evolution of the perturbations is invariant under this exchange. We must remember, however, that in the first and last regions we need to force $C_1=0$ and $B_N=0$, respectively, and the resulting equations which we have written explicitly in Eq. (22) break this symmetry, *unless* $\rho_1=\rho_N=0$. We conclude that if the central sphere is a vacuum ($\rho_1=0$) and the outermost shell is also a vacuum ($\rho_N=0$), then the perturbations in an arbitrary number of shells evolve in such a way as to be symmetric between n and $-n-1$.

Of course this symmetry does not appear for the classical $N=2$ case (unless both fluids have zero density!). It is valid for a shell or series of shells bounded by vacuum on the inside and on the outside.

We now turn to two simple systems: $N=2$ and 3.

III. $N=2$ CASE

A. Analytical results

We have seen that when there are N fluids they have $N-1$ interfaces and an equal number of evolution equations given by Eq. (20). For $N=2$ we have only one equation because there is only one interface between a central fluid of density ρ_1 and an outer fluid of density ρ_2. We will simplify our notation in this section by defining $R\equiv R_1(t)$ and $\eta\equiv\eta_1(t)$ since there is only one interface position and one perturbation amplitude.

Equation (20) reduces to Eqs. (22a) and (22b) for the first and last interfaces, respectively. These interfaces coincide for $N=2$, hence we can use either Eq. (22a) or (22b). The latter equation reads

$$(\rho_2-\rho_1)\frac{d}{dt}(R^2\dot{R}\eta) =-\rho_1\left[R^{n+2}\frac{dB_1}{dt}+(n\rightarrow -n-1)\right] +\rho_2R^{-n+1}\frac{dC_2}{dt}\ , \quad (26)$$

with $nB_1=-R^{-n-1}d(R^2\eta)/dt$ and $(n+1)C_2=R^nd(R^2\eta)/dt$ [see Eq. (23)]. Substituting these expressions in the above equation and collecting terms, we obtain Plesset's equation

$$\frac{d^2\eta}{dt^2}+3\frac{\dot{R}}{R}\frac{d\eta}{dt}-nA(n)\frac{\ddot{R}}{R}\eta=0\ , \quad (27)$$

with

$$nA(n)=\frac{n(n-1)\rho_2-(n+1)(n+2)\rho_1}{n\rho_2+(n+1)\rho_1} \quad (28a)$$

$$=\frac{(n^2+n+1)A-2n-1}{n+(1-A)/2}\ . \quad (28b)$$

As we mentioned earlier, the coefficient $nA(n)\rightarrow nA$ in the large-n limit, where A is the Atwood number $(\rho_2-\rho_1)/(\rho_2+\rho_1)$. Of course for $A=1$ ($\rho_1=0$) we get $nA(n)=n-1$ and we recover Eq. (1).

An alternative form of Eq. (27) is

$$\frac{1}{R^3}\frac{d}{dt}\left[R^3\frac{d\eta}{dt}\right]-nA(n)\frac{\ddot{R}}{R}\eta=0\ , \quad (29)$$

which is sometimes useful when we seek solutions to Plesset's equation.

We now consider analytic solutions. As far as we know there is no general solution, by which we mean a solution $\eta(t)$ to Eq. (27) or (29) for an arbitrary implosion or explosion history $R(t)$, arbitrary densities ρ_1 and ρ_2, and arbitrary mode number n [of course only the combination $nA(n)$ matters in Plesset's equation]. We are therefore led to consider two classes of solutions which we denote as class A and class B. Class-A solutions are valid for specific values of $nA(n)$ but arbitrary histories $R(t)$; class-B solutions are the reverse: valid for arbitrary $nA(n)$, but only specific $R(t)$. Of course the doubly restricted case where both $nA(n)$ and $R(t)$ are specified can be obtained as a special case of either class. This will serve as a nontrivial check of our analytic as well as numerical solutions.

We have found only two class-A solutions: (i) $nA(n)=-2$, in which case the solution is

$$\eta(t)=\eta_0(R_0/R)^2+\frac{2\dot{R}_0\eta_0+R_0\dot{\eta}_0}{R^2}\int_0^t R(t)dt\ , \quad (30)$$

and (ii) $nA(n)=0$, in which case the solution is

$$\eta(t)=\eta_0+\dot{\eta}_0\int_0^t(R_0/R)^3dt\ . \quad (31)$$

There are two distinct situations which lead to the first case with $nA(n)=-2$: one is $n=0$ with arbitrary ρ_1 and ρ_2 as we reported earlier.[12] The other is $\rho_1=\rho_2$ with arbi-

trary n, in which case there is no density mismatch and the distortions are geometric in origin.

The second case with $nA(n)=0$ is perhaps more interesting because if $\dot{\eta}_0=0$ then $\eta(t)=\eta_0$ [see Eq. (31) above], i.e., the amplitude does not grow or diminish no matter what one chooses for the radial history $R(t)$. We will refer to such modes as "critical modes." From Eq. (28b) these modes satisfy the relation $(n^2+n+1)A-2n-1=0$ and therefore

$$n_{\text{critical}}=\frac{2-A+(4-3A^2)^{1/2}}{2A} . \tag{32}$$

Alternatively, one can define A_{critical}:

$$A_{\text{critical}}=\frac{1+2n}{1+n+n^2} , \tag{33}$$

for any given mode number n. For example, $A_{\text{critical}}=1$ if $n=1$ and $A_{\text{critical}}=\frac{7}{13}$ for $n=3$, etc. As n increases, A_{critical} approaches zero. We can view the critical modes as perturbations which do not grow because the pressure forces arising from the density mismatch are exactly balances by the purely geometrical distortions.

We now turn to class-B solutions which are valid for arbitrary $nA(n)$ but specific $R(t)$. We have found analytic class-B solutions for the following four cases: (i)

$$R=R_0e^{t/T} ,$$

(ii)

$$R=R_0(1+t/T)^{1/3} ,$$

(iii)

$$R=R_0+\dot{R}_0t+\tfrac{1}{2}gt^2 ,$$

and (iv)

$$\ddot{R}=\Delta v\delta(t-t_s) .$$

The solutions to these four cases are discussed in the Appendix in detail.

The last two cases can be referred to as a constant acceleration and a shock, respectively, hence they are the familiar Rayleigh-Taylor[1] (RT) and the Richtmyer-Meshkov[2] (RM) instabilities in spherical geometry. The solution for the RT case is given in terms of hypergeometric functions [see the Appendix, Eq. (A15)] and *not* by an exponential as was erroneously assumed by Gupta and Lawande.[6,11] For the RM case the solution is

$$\eta(t)=\eta_0\left\{1+\frac{nA(n)}{2}\left[1-\left[\frac{R_0}{R}\right]^2\right]\right\} , \tag{34}$$

where we have assumed that $\dot{\eta}_0=0$ before the shock which arrives at $t=0$.

Shock-induced implosions and explosions can be treated in a unified manner by writing $R=R_0(1+t/T)$, where a positive (negative) time constant T corresponds to an explosion (implosion). Since

$$1-(R_0/R)^2=t(t+2T)/(t+T)^2 , \tag{35}$$

we conclude from Eqs. (34) and (35) that the perturbations evolve linearly with time as long as $t\ll|T|$. If the interface was moving prior to the shock and if the shock *stops* the radial motion then we find that perturbations at such a stationary interface evolve linearly with time for all t (see the Appendix).

As in plane geometry shocks can induce phase reversal of perturbations (see Meshkov[2]). Clearly, $\eta(t)$ in Eq. (34) goes through zero and changes sign if $nA(n)$ is positive and $R<R_0$ (implosion), or if $nA(n)$ is negative and $R>R_0$ (explosion). In either case the phase change occurs at

$$R=R_0\left[1+\frac{2}{nA(n)}\right]^{-1/2} \tag{36}$$

independently of η_0. For example, if $nA(n)=50$ then the amplitude goes through zero after the radius has moved in only 2%, i.e., $R/R_0=(\frac{25}{26})^{1/2}\approx 98\%$.

Finally, the phenomenon of freeze-out occurs in spherical as in planar geometry.[5] By appropriately timing a second shock one can stop the growth of perturbations, i.e., set $\eta(t)=$const, as we discuss in the Appendix.

B. Numerical examples

We will consider a system which implodes from an initial radius $R_0=25R_f$ to a final radius R_f. The ratio R_0/R_f is also called the "convergence ratio." Two types of implosions will be considered: a constant acceleration and deceleration, and an exponential acceleration. The second example can of course be solved analytically [see Eq. (A2)], and we considered it first as a test problem to check our numerical integration of Plesset's equation and, second, to see how the evolution of the perturbation depends on the implosion history $R(t)$. The initial and final radii were the same in both implosions, and so was the implosion time.

Our units for distance and time are fixed by setting the final radius equal to 1 and the implosion time equal to 8. Since $R=R_0e^{t/T}$ for the exponential implosion, the time constant is given by $T=-8/\ln 25$. For the constant acceleration and deceleration case we chose a negative acceleration $(-\frac{3}{2})$ for the first 4 time units and a positive $(+\frac{3}{2})$ acceleration for the remaining time. In this way the radius cover 12 units in the first half of the implosion and another 12 units in the second half to go from the initial value of 25 to the final value of 1. Figures 2(a)–2(c) show the radius, the velocity, and the acceleration for each type of implosion.

A numerical example will clarify these points. A shell with an initial radius 2.5 mm moves in with a constant acceleration of 150 μm/ns^2 for a period of 4 ns, during which time it covers 1200 μm and reaches an implosion velocity of 600 μm/ns. In the next 4 ns it decelerates at 150 μm/ns^2 and comes to rest after covering another 1200 μm, hence $R_f=100$ μm.

We next specify the density ratio ρ_2/ρ_1 and mode number n, which we do for two sets of numbers. Let us first take $\rho_2/\rho_1=10$ and $n=50$; such large density contrasts and mode numbers are relevant to ICF implosions. Of course the controlling quantity is $nA(n)$ which is

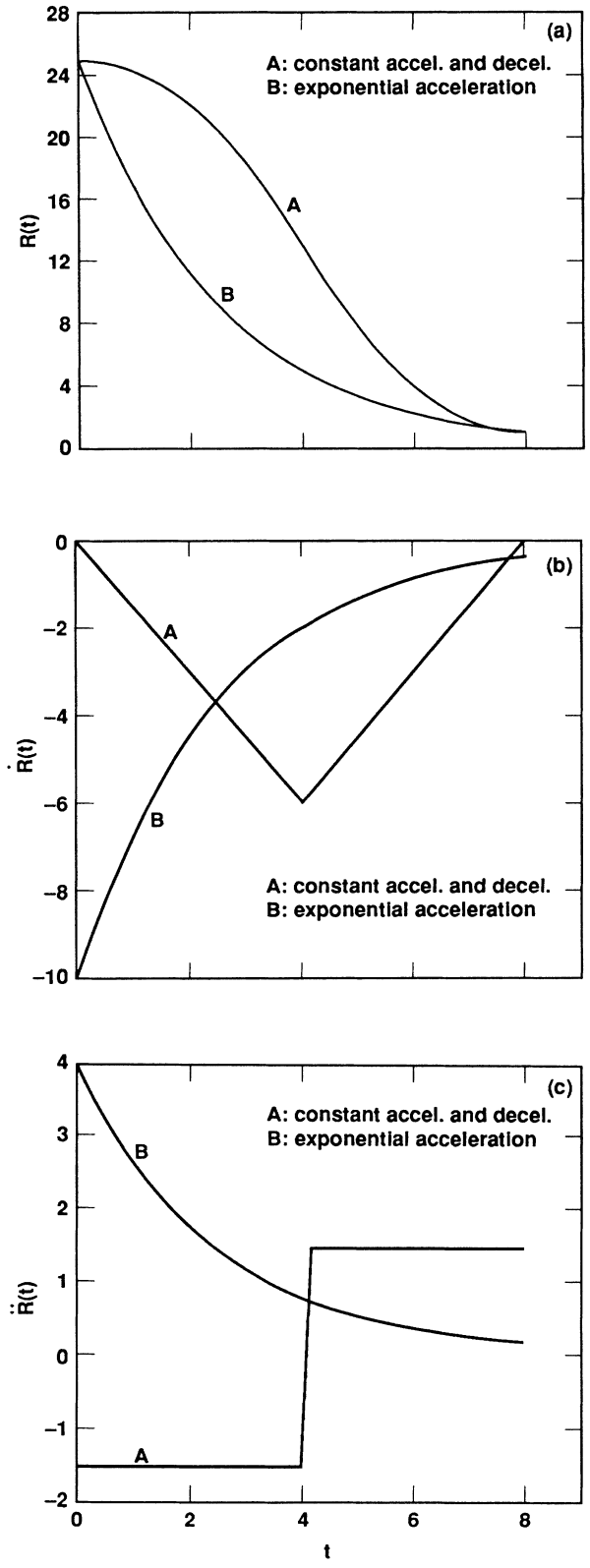

FIG. 2. (a) The radius, (b) the radial velocity, and (c) the radial acceleration of the interface in a two-fluid imploding system. Curves labeled A describe a constant acceleration and deceleration, and curves labeled B describe an exponential acceleration. For both types of implosions the radius goes from 25 to 1 in 8 times units (see text).

$21848/551 \approx 40$ for this case—other combinations of ρ_2/ρ_1 and n yielding the same $nA(n)$ will evolve identically.

The evolution of the perturbations for each type of implosion is shown in Fig. 3. Note that η grows exponentially in time when the implosion itself, i.e, $R(t)$, is exponential in time (curves labeled B in Figs. 2 and 3). The constant acceleration case first oscillates because $Ag < 0$ during $0 < t < 4$, and then grows, somewhat faster than exponentially, during the deceleration phase $4 < t < 8$. Only absolute values are graphed on semilogarithmic plots. In all our numerical results we set $\eta_0 = 1$ and $\dot{\eta}_0 = 0$.

As Fig. 3 shows, the two different ways A and B of getting from $R_0 = 25$ to $R_f = 1$ give substantially different perturbation growth, suggesting that it might be possible to shape the pulse of a laser drive on an ICF capsule in an effort to reduce the growth of perturbations. To actually achieve such a reduction via pulse shaping one must take into account the effects of compressibility, radiation, heat conduction, and ablation. Direct numerical simulations will be required for this purpose, as we discuss briefly in Sec. VI.

Keeping the same implosion histories and initial conditions, we now consider a second set of density ratios and mode numbers to illustrate the critical modes. Specifically, let $\rho_2/\rho_1 = \frac{22}{15}$ and consider three values for n: $n = 9$, 10, and 11. The critical mode satisfying $nA(n) = 0$ is $n = 10$ for this density ratio. Whether the implosion history is the constant acceleration and deceleration case

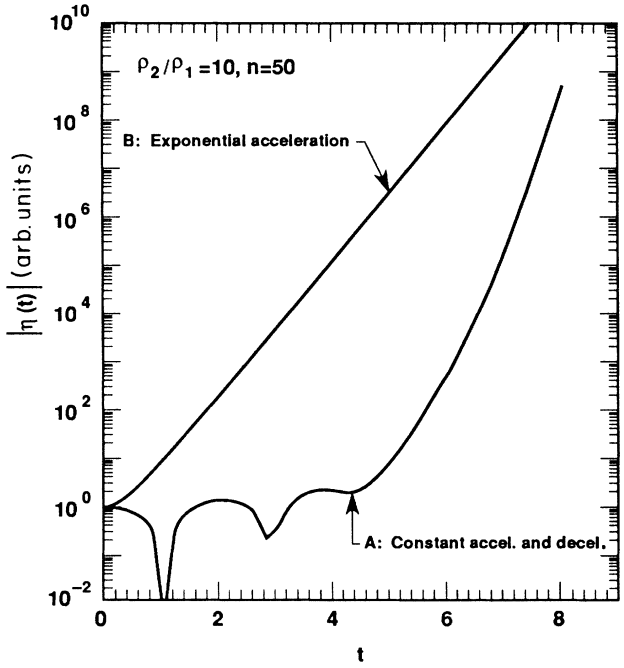

FIG. 3. The magnitude of the perturbation amplitude $|\eta(t)|$ vs time for the constant acceleration and deceleration case A and the exponential acceleration case B shown in Fig. 2. The initial conditions read $\eta_0 = 1$ and $\dot{\eta}_0 = 0$. The constant $nA(n) = \frac{21848}{551} \approx 40$.

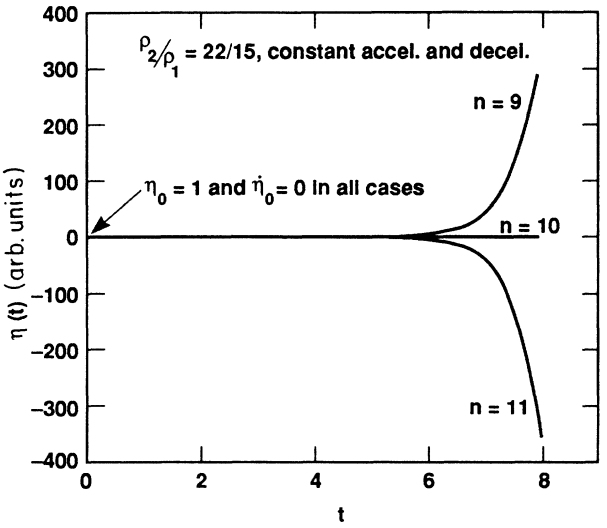

FIG. 4. The perturbation amplitude $\eta(t)$ vs time for the constant acceleration case (curves labeled A in Fig. 2). The density ratio is $\rho_2/\rho_1=\frac{22}{15}$ and three modes are shown: $n=9$, 10, and 11. The mode $n=10$ is a "critical mode," i.e., $nA(n)=0$, and therefore does not grow. Initial conditions read $\eta_0=1$ and $\dot{\eta}_0=0$.

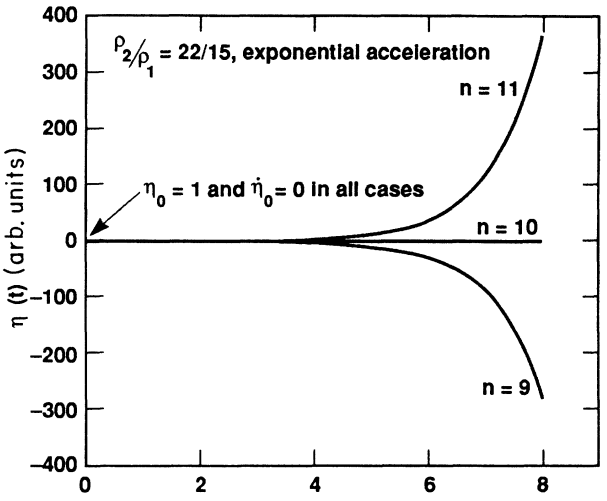

FIG. 5. Same as Fig. 4 for the exponentially imploding case.

(Fig. 4) or the exponential case (Fig. 5), the critical mode does not grow while the two adjacent modes $n=9$ and 11 exhibit a healthy growth. Such behavior, viz., absolute stability of critical modes for any implosion or explosion history, can serve as a good test problem for two-dimensional (2D) or 3D numerical codes.

IV. $N=3$ CASE

A. Analytical results

For the three-fluid case there are two interfaces: the first at $r=R_1$ and the second at $r=R_2$. As mentioned in Sec. II, the general evolution equation, Eq. (20), must be augmented by $C_1=0$ in the first region and $B_N=0$ in the last region [the C_i are the terms denoted by $(n\rightarrow -n-1)$ in Eq. (20)]. Equations (22a) and (22b) give the evolution of the perturbations at the first and last interfaces which are the only two interfaces for $N=3$:

$$(\rho_2-\rho_1)\frac{d}{dt}(R_1^2\dot{R}_1\eta_1) = R_1^{n+2}\rho_2\frac{dB_2}{dt}+(n\rightarrow -n-1)-R_1^{n+2}\rho_1\frac{dB_1}{dt}\ , \tag{37a}$$

$$(\rho_3-\rho_2)\frac{d}{dt}(R_2^2\dot{R}_2\eta_2) = -\rho_2\left[(R_2)^{n+2}\frac{dB_2}{dt}+(n\rightarrow -n-1)\right] +\rho_3(R_2)^{-n+1}\frac{dC_3}{dt}\ , \tag{37b}$$

with

$$B_1=-\frac{1}{nR_1^{n+1}}\frac{d}{dt}(R_1^2\eta_1)\ , \tag{38a}$$

$$B_2=\frac{-(R_2)^{-n-1}}{n[1-(R_1/R_2)^{2n+1}]}\frac{d}{dt}(R_2^2\eta_2) +(R_1\rightleftharpoons R_2,\eta_1\rightleftharpoons\eta_2)\ , \tag{38b}$$

$$C_3=\frac{R_2^n}{n+1}\frac{d}{dt}(R_2^2\eta_2)\ , \tag{38c}$$

where we have used Eq. (14), (23a) and (23b) with $N=3$.

When the middle shell is very thick, i.e., $R_2\gg R_1$, Eqs. (37a) and (37b) decouple and we obtain two $N=2$ equations, one for each interface. If we set $\rho_2=0$, Eqs. (37a) and (37b) again decouple and reduce to two $N=2$ equations with appropriate values of $nA(n)$: $nA(n)=-n-2$ and $nA(n)=n-1$ for Eq. (37a) and (37b), respectively. The algebra is simplified by noting that an alternative form of the $N=2$ (i.e., Plesset's) equation is

$$\frac{d}{dt}\left[\frac{1}{R}\frac{d}{dt}(R^2\eta)\right]-[2+nA(n)]\ddot{R}\eta=0\ . \tag{39}$$

When the middle fluid has a finite thickness and a nonzero density Eqs. (37a) and (37b) remain two coupled second-order linear differential equations which, in general, must be solved numerically.

An interesting case is the spherical analog of the planar problem considered by Taylor:[1] $\rho_1=\rho_3=0$. Equations (37a) and (37b) reduce to

$$\frac{d}{dt}(R_1^2\dot{R}_1\eta_1)=(R_1)^{n+2}\frac{dB_2}{dt}+(n\rightarrow -n-1)\ , \tag{40a}$$

$$\frac{d}{dt}(R_2^2\dot{R}_2\eta_2)=(R_2)^{n+2}\frac{dB_2}{dt}+(n\rightarrow -n-1)\ , \tag{40b}$$

which are, as expected, independent of the density ρ_2 of

the middle shell and are symmetric under $n \Longleftrightarrow -n-1$.

We now consider the thin-shell limit which turns out to be nontrivial for the following reason: from mass or volume conservation we have $R_1^2\dot{R}_1 = R_2^2\dot{R}_2$; as $R_2 \to R_1$, Eq. (40) implies that $\eta_2 \to \eta_1$. If we define a shell thickness ΔR and an average radius R by

$$\Delta R = R_2(t) - R_1(t), \quad R = [R_2(t) + R_1(t)]/2 , \tag{41}$$

then to lowest order in $\Delta R/R$ we must keep terms of order $(\eta_2 - \eta_1)/\Delta R$. The algebra is quite tedious and we will omit the details. The final result is

$$\frac{d^2}{dt^2}(\eta_2 + \eta_1) = -2\frac{\ddot{R}}{\Delta R}(\eta_2 - \eta_1) , \tag{42a}$$

$$\frac{d^2}{dt^2}\left[\frac{R}{\Delta R}(\eta_2 - \eta_1)\right] = \ddot{R}\left[3\frac{(\eta_2 - \eta_1)}{\Delta R} - (n+2)(n-1)\frac{(\eta_2 + \eta_1)}{2R}\right] . \tag{42b}$$

Remarkable cancellations occur leading to the above two simple equations. Note that $\dot{R}$ does not appear explicitly. Also, the mode number n appears only in the combination $(n+2)(n-1)$ which of course is symmetric under $n \Longleftrightarrow -n-1$, providing a nontrivial check of our calculation. One might be tempted to drop the last term which is proportional to $(\eta_2 + \eta_1)/R$; however, it multiplies $(n+2)(n-1)$ which can be very large for large n. No simplifying assumptions about n or about the radial history $R(t)$ were made in deriving Eqs. (42a) and (42b). They are valid for $\Delta R/R \ll 1$. We must warn the reader that it is possible for an initially thin shell to thicken up by geometric convergence so much that during the final stages of an implosion the shell is as large or larger than the average radius, in which case the condition $\Delta R/R \ll 1$ is violated and one must revert back to Eqs. (40a) and (40b).

Defining

$$\Delta\eta = \eta_2 - \eta_1, \quad \eta = (\eta_2 + \eta_1)/2 , \tag{43}$$

Eqs. (42a) and (42b) read

$$\frac{d^2\eta}{dt^2} = -\frac{\ddot{R}}{\Delta R}\Delta\eta , \tag{44a}$$

$$\frac{d^2}{dt^2}\left[\frac{R\Delta\eta}{\Delta R}\right] = \ddot{R}\left[3\frac{\Delta\eta}{\Delta R} - (n+2)(n-1)\frac{\eta}{R}\right] . \tag{44b}$$

We will consider only two cases: a constant radial velocity and a shock. For the constant $\dot{R}$ case we have $\ddot{R} = 0$, $R = R_0 + \dot{R}_0 t = R_0(1 + t/T)$, where $T > 0$ $(T < 0)$ for an explosion (implosion), and Eqs. (44a) and (44b) can be easily solved:

$$\eta(t) = \eta_0 + \dot{\eta}_0 t , \tag{45a}$$

$$\left[1 + \frac{t}{T}\right]^3 \Delta\eta = \Delta\eta_0\left[1 + \frac{3t}{T}\right] + \Delta\dot{\eta}_0 t , \tag{45b}$$

where we have used the fact that for a thin shell $R/\Delta R \sim R^3/(\Delta R_0 R_0^2) \sim (1 + t/T)^3$. Note that only the difference in amplitudes $\eta_2 - \eta_1$ is affected by the nature of the radial motion, i.e., implosion versus explosion; the sum $\eta_2 + \eta_1$ is independent of T. Furthermore, if $\dot{\eta}_1(0) = \dot{\eta}_2(0) = 0$, i.e., $\dot{\eta}_0 = \Delta\dot{\eta}_0 = 0$, then $\eta(t) = \eta_0$ so that the sum $\eta_2 + \eta_1$ does not grow or diminish at all, though the difference $\eta_2 - \eta_1$ evolves with time. If the shell is imploding then this difference goes through zero and changes phase at $t = |T|/3$ when the shell is $\frac{2}{3}$ of the way in, i.e., $R = \frac{2}{3}R_0$. If the shell is exploding then the difference $\eta_2 - \eta_1$ maintains its sign and never goes through zero. We repeat that, in either case, implosion or explosion, the sum $\eta_2 + \eta_1$ remains constant.

We now turn to a shock and let $\ddot{R} = \Delta v\,\delta(t)$ where $\Delta v = \dot{R}(0_+) - \dot{R}(0_-) \equiv \dot{R}_+ - \dot{R}_-$. Integrating Eqs. (44a) and (44b) over $0_- < t < 0_+$ and noting that variables such as η, R, $\Delta\eta$, and ΔR do not change instantaneously while their derivatives do, we get

$$\dot{\eta}_+ = \dot{\eta}_- - \frac{\Delta v}{\Delta R_0}\Delta\eta_0 , \tag{46a}$$

$$\Delta\dot{\eta}_+ = \Delta\dot{\eta}_- - (n+2)(n-1)\eta_0\Delta v\frac{\Delta R_0}{R_0^2} . \tag{46b}$$

We have used the relation

$$\frac{d}{dt}(R/\Delta R) \approx 3(\dot{R}/\Delta R), \quad \Delta R \ll R$$

to cancel a term in the rhs of Eq. (44b) against an identical term in the left-hand side (lhs) of that equation when we integrate it over time.

If the motion starts first with a shock, then the shock sets the initial conditions for the subsequent evolution of the amplitudes. For example, if the motion starts with a shock at $t = 0$ followed by a constant radial velocity, we combine Eqs. (45) and (46) to get

$$\eta(t) = \eta_0 - \Delta\eta_0\frac{\Delta v}{\Delta R_0}t , \tag{47a}$$

$$\left[1 + \frac{t}{T}\right]^3 \Delta\eta = \Delta\eta_0\left[1 + \frac{3t}{T}\right] - (n+2)(n-1)\eta_0\Delta v\frac{\Delta R_0}{R_0^2}t . \tag{47b}$$

A second shock may arrive at a later time. As in the $N = 2$ case the second shock, if properly timed, can freeze-out some of the perturbations. There are too many possibilities for the $N = 3$ case and the analysis becomes quite complicated. We mention only that it is *not* possible for the second shock to freeze out the perturbations at *both* interfaces.

B. Numerical examples

We now consider two numerical examples: (i) an imploding shell and (ii) an exploding shell. We have written a code that solves the fully coupled equations (37a) and (37b) for arbitrary densities, shell thicknesses, and radial histories. Note that only one of the two interfaces, e.g.,

$R_1(t)$, can be arbitrary—the other is fixed by the conservation of the mass (or the volume) of the shell:

$$R_2(t)=[R_2^3(0)-R_1^3(0)+R_1^3(t)]^{1/3}\ , \tag{48a}$$

which gives the familiar relation

$$\dot{R}_2=(R_1/R_2)^2\dot{R}_1\ , \tag{48b}$$

and

$$\ddot{R}_2=\left[2R_1\left[1-\frac{R_1^3}{R_2^3}\right]\dot{R}_1^2+R_1^2\ddot{R}_1\right]\Big/R_2^2\ . \tag{48c}$$

For our examples we chose $(\rho_1,\rho_2,\rho_3)=(1,\ 10,\ 1)$. As we mentioned earlier, such high-density contrasts are relevant to ICF.

(i) *Implosion.* For the implosion history we chose $R_1(t)$ to follow the constant acceleration and deceleration history considered in Sec. III: R_1 has an initial value of 25, accelerates inwards for 4 time units, decelerates for another 4 units and comes to rest at a final radius of 1. The only free parameter for R_2 is its initial value $R_2(0)$ or, equivalently, the initial shell thickness, which we chose to be 1. The ratio $R_1(0)/[R_2(0)-R_1(0)]$ is also known as the "aspect ratio." For our example, the aspect ratio and the convergence ratio are both 25. In Fig. 6 we show the radius, the velocity, and the acceleration of both interfaces. Note that the final conditions read $R_2=(1952)^{1/3}\approx 12.5$ (final shell thickness approximately equal to 11.5). This is an example of how an initially thin shell with $\Delta R/R=\frac{1}{25}\ll 1$ thickens up by convergence to $\Delta R/R\approx\frac{11}{6}\frac{5}{75}>1$, as we mentioned in our discussion of thin shells.

Figure 7 shows the evolution of the perturbations at each interface. In all our numerical work we set $\dot{\eta}_{1,2}(0)=0$, and consider finite initial amplitudes at one or both of the interfaces. We set $(\eta_1,\eta_2)_0=(1,0)$, (0,1), and (1,1) in Figs. 7(a), 7(b), and 7(c), respectively.

We see that in all cases the perturbation on the inner surface grows much larger than the perturbation at the outer surface. This occurs during the deceleration phase of the implosion, i.e., after $t>4$, when the lower-density inner fluid ($\rho=1$) decelerates the shell ($\rho=10$). In fact, the evolution of $\eta_1(t)$ is not much different between this $N=3$ case and the $N=2$ case considered in Sec. III. On the other hand, the perturbation $\eta_2(t)$ at the outer surface grows only during the earlier acceleration phase ($t<4$) when the lower-density outer fluid "pushes" on the shell. Qualitatively, such behavior is expected from classical and planar considerations according to which instability (stability) occurs when $Ag>0$ ($Ag<0$).

The mode number n was taken to be 50 in the above examples. We obtained similar results with other values of n. For example, with $n=100$ the early time oscillations of η_1 were faster and its late time growth was larger, as expected.

Figures 7(a) and 7(b) illustrate also the phenomenon of feedthrough,[4] particularly at early times when the shell is thin: the interfaces are coupled to each other in such a way that a perfectly smooth surface with no initial perturbation acquires a finite perturbation amplitude from a

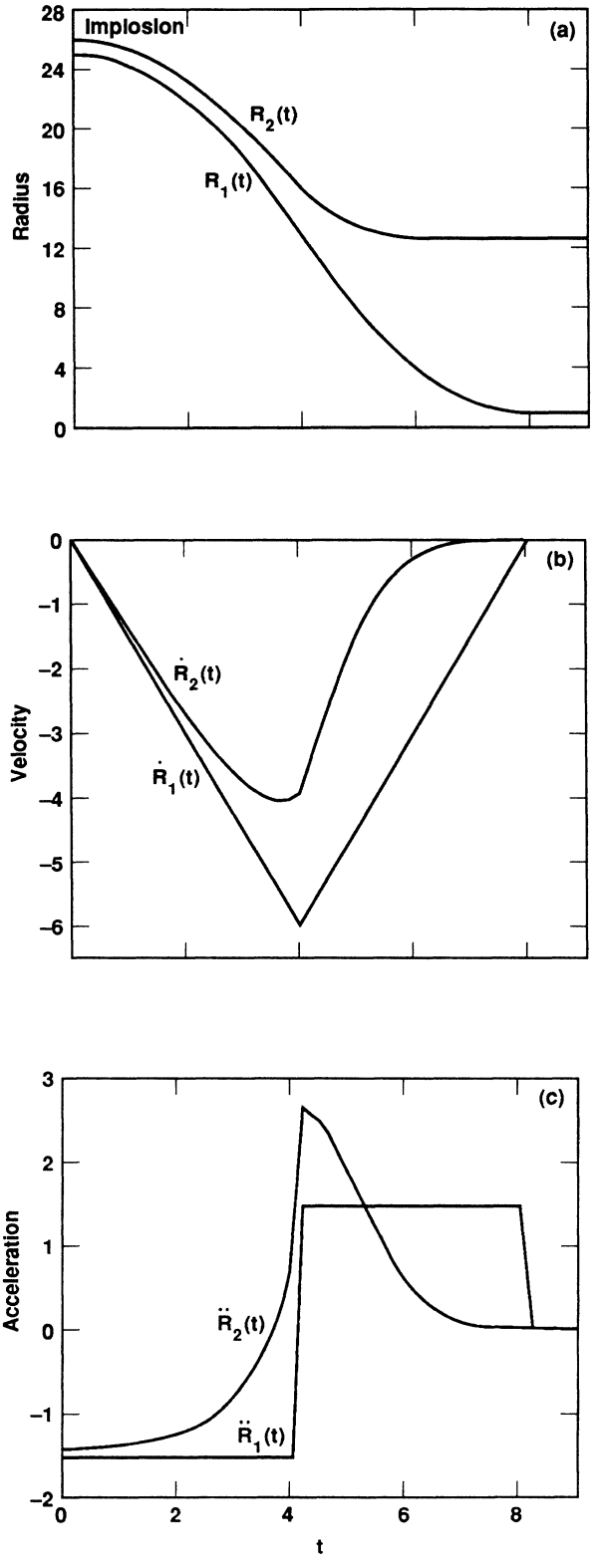

FIG. 6. (a) The radius, (b) the radial velocity, and (c) the radial acceleration of a shell imploding with a constant acceleration and/or deceleration. $R_1(t)$ and $R_2(t)$ refer to the inner and outer radii of the shell which is initially 1 unit thick. The inner radius $R_1(t)$ moves from an initial value of 25 to a final value of 1. $R_2(t)$ is obtained via mass conservation. For units see text.

neighboring perturbed interface and that amplitude can later grow very large. Note that during the later stages of the implosion there is much less feedthrough: while $\eta_1(t)$ is growing $\eta_2(t)$ remains at its relatively small value of 200–2000. The reason is that the shell has thickened up [see Fig. 6(a)] and the interfaces are separated further: the ratio R_1/R_2 which initially is $\frac{25}{26}\approx 1$ decreases to approximately $\frac{1}{10}$ during the second half of the implosion. Since the coupling is of order $(R_1/R_2)^n$, for $n=50$ it becomes much less effective in the later stages. We verified this by running other n values and finding that the low-n modes couple more efficiently than high-n modes. The same phenomenon occurs in plane geometry where $(R_1/R_2)^n \rightarrow e^{-k\Delta R}$, $k=2\pi/\lambda$—longer wavelengths couple more efficiently than shorter wavelengths.

The results shown in Fig. 7 were not changed in any substantial way when we set $(\rho_1,\rho_2,\rho_3)=(0,10,0)$ and/or $n=-51$. The large ratio of densities, viz., 10 to 1, in the original set (1,10,1) implies that the results are not affected much by zeroing out ρ_1 and ρ_3. For $\rho_1=\rho_3=0$ we obtained identical results when we set $n=50$ or -51 in our numerical code, which is a nontrivial check of the integration routine. Even with the original set (1,10,1) the results between $n=50$ and -51 were similar because of the large 10-to-1 density ratio which favors the contribution of the ρ_2 terms in Eq. (37). We naturally expect that $n \Longleftrightarrow -n-1$ will be a good symmetry when the density ratios at the first and last interfaces, ρ_1/ρ_2 and ρ_N/ρ_{N-1}, are small but not necessarily zero.

(ii) *Explosion.* To illustrate an exploding shell we chose to reverse the implosion described above: we start with a shell of outer radius $(1952)^{1/3}\approx 12.5$ and inner radius $R_1(0)=1$. $R_1(t)$ accelerates outwards for 4 time units then decelerates for another 4 times units until it stops, at $t=8$, at a radius of 25, by which time R_2 is at 26, i.e., the initially thick shell ends up 1 unit thick via mass conservation. The exploding motion is shown in Fig. 8. In this way the initial conditions for one type of motion serve as final conditions for the other, and vice versa.

For the same densities (1,10,1) and mode number $n=50$ we show in Fig. 9 the evolution of the perturbations at the inner and outer surfaces of the exploding shell. Three initial conditions were considered as before: $(\eta_1,\eta_2)_0=(1,0)$, (0,1), and (1,1) in Figs. 9(a), 9(b), and 9(c), respectively. All started with $\dot{\eta}_{1,2}(0)=0$.

There are several distinct differences between the imploding shell (Fig. 7) and the exploding shell (Fig. 9). The most obvious is the scale: 10^6 for explosions compared with the previous 10^{10} for implosions. Another difference is that the final amplitudes η_1 and η_2 are comparable here. This is a result of feedthrough: the exploding shell becomes thinner $(11.5\rightarrow 1)$ so that the perturbations at one interface are essentially replicated at the other. Finally, the initial conditions $(\eta_1,\eta_2)_0=(1,0)$ and (1,1) yield essentially identical results [compare Figs. 9(a) and 9(c)], while the (0,1) condition, Fig. 9(b), exhibits extremely inhibited growth—only a factor of 100, which is four orders of magnitude less than the growth factors of Figs. 9(a) and 9(c). This behavior can be understood by feedthrough: in the (0,1) case η_2 oscillates during the

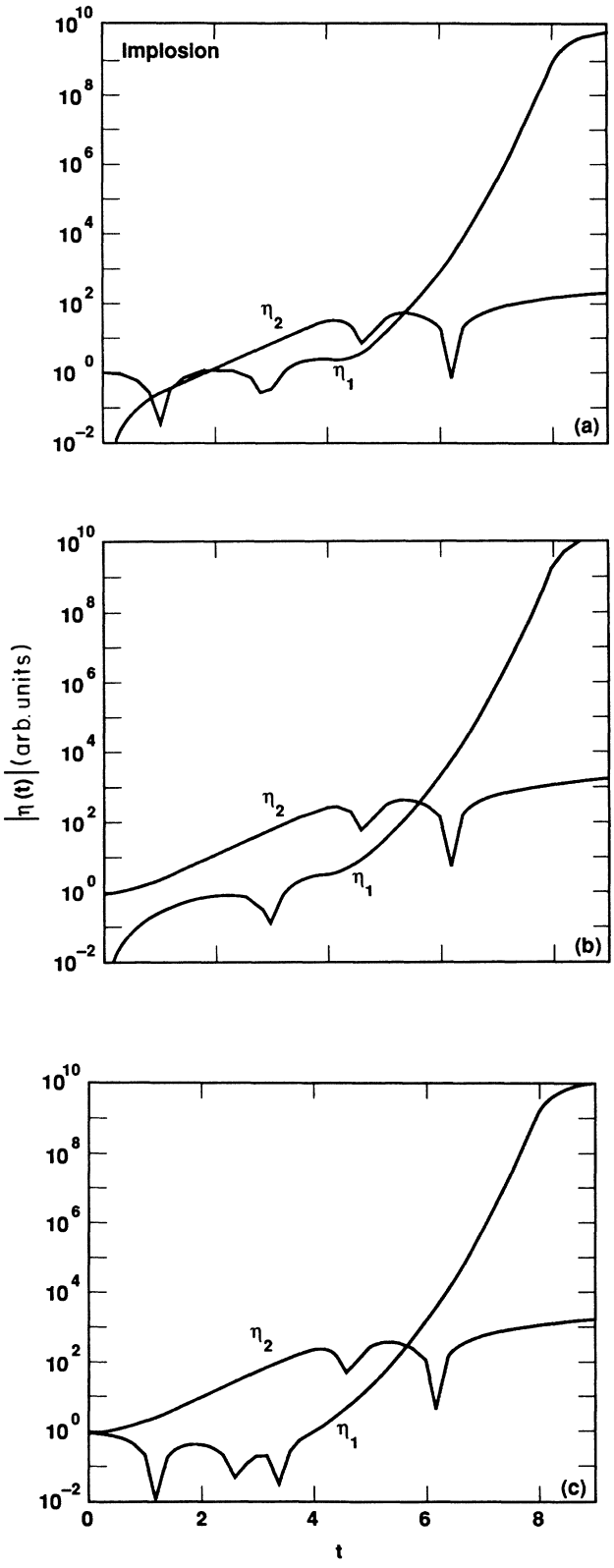

FIG. 7. The perturbation amplitudes $\eta_1(t)$ and $\eta_2(t)$ at the inner and outer surfaces of the imploding shell as shown in Fig. 6. Only absolute values are plotted, and the scale is arbitrary. The initial conditions read $(\eta_1,\eta_2)_0=(1,0)$, (0,1), and (1,1) in (a), (b), and (c), respectively.

time $t \leq 4$—it is classically stable because $Ag < 0$. Since the shell is initially thick, there is little feedthrough to the inner surface which is highly unstable. After $t = 4$ the outer surface does become unstable and perturbations grow there, albeit by a factor of only 100 (note that the acceleration at the outer surface is generally less than the acceleration at the inner surface). During this phase ($t > 4$) the inner surface is "stable," but the shell is thin enough that perturbations feed through from the outer to the inner surface inducing some relatively small perturba-

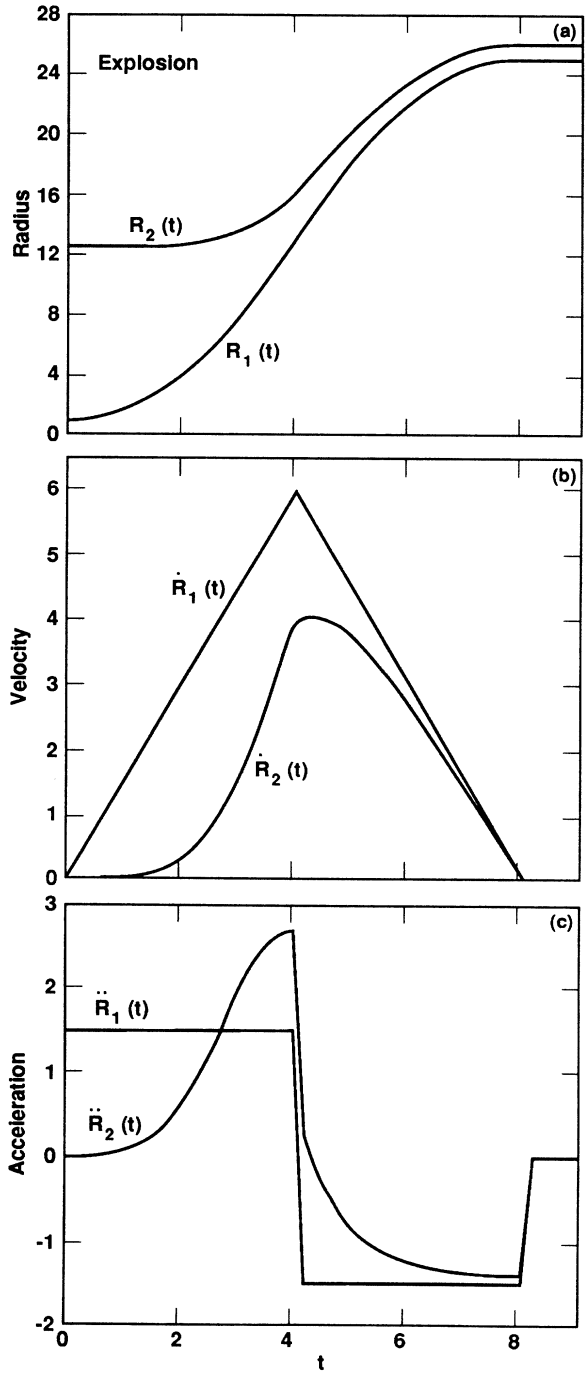

FIG. 8. (a) The radius, (b) the radial velocity, and (c) the radial acceleration of a shell exploding with a constant acceleration and deceleration. $R_1(t)$ and $R_2(t)$ refer to the inner and outer radii of the shell. Their initial values are 1 and $(1952)^{1/3} \approx 12.5$, respectively (the shell starts ~ 11.5 units thick). Their final values are $R_1 = 25$ and $R_2 = 26$ (shell 1 unit thick). This explosion is the mirror image of the implosion shown in Fig. 6.

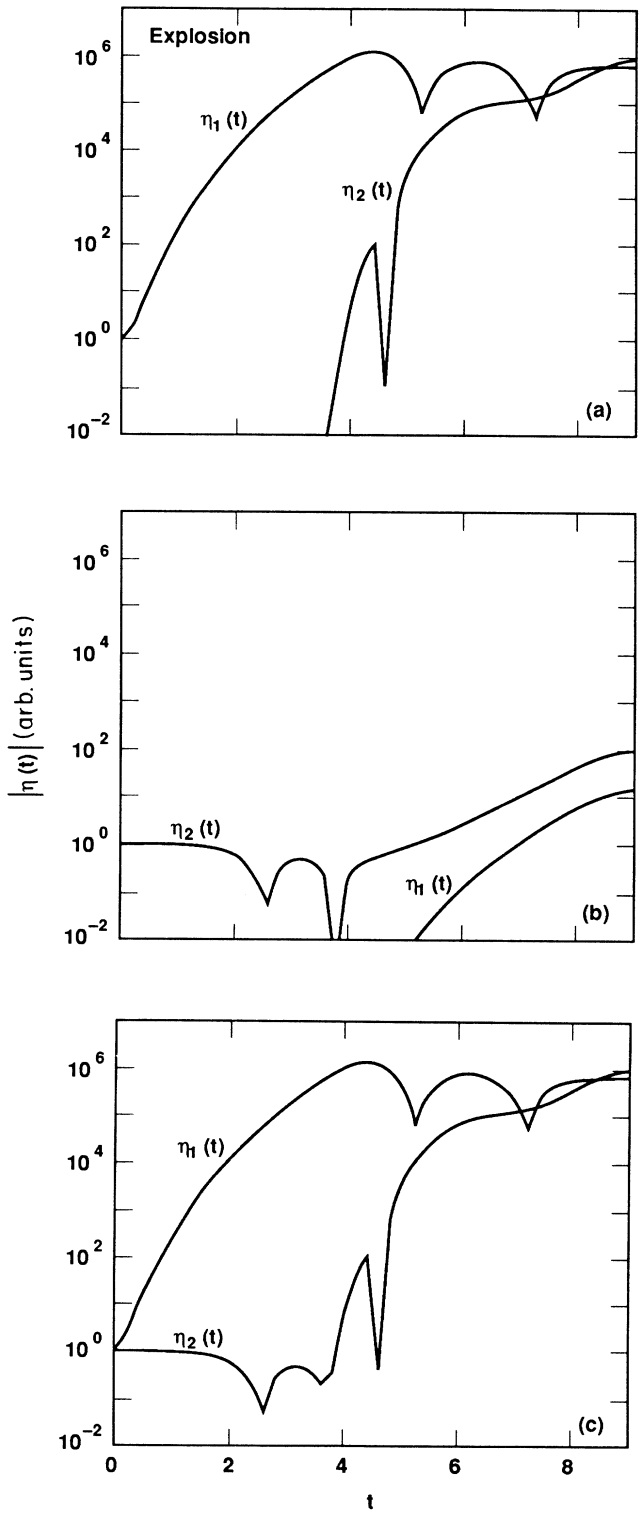

FIG. 9. Same as Fig. 7 for the exploding shell.

tions at that inner surface. Figures 9(a) and 9(c), which exhibit a completely different evolution, can also be explained by the same phenomenon of feedthrough. For example, in Fig. 9(c) the early large growth of $\eta_1(t)$ is *not* replicated by η_2 because the shell is thick. It *is* replicated later when the shell becomes thin, so much so that one can notice η_2 mimicking the late time oscillations of η_1. In itself, η_2 is unstable and would have grown uniformly, albeit slowly , were it not for the close proximity of the highly perturbed inner surface with its large (10^6) and oscillating perturbation η_1. We checked this explicitly: we multiplied $\eta_1(0)$ by a certain factor (10^{-3}) without changing $\eta_2(0)$. We found that this factor was carried through by not only η_1 but η_2 also exhibited the same factor at late times. The fact that η_2 was affected in direct proportion to η_1 is an unambigous sign of feedthrough.

The dramatic smallness of the perturbations in Fig. 9(b) is a combination of four factors all of which are favorable: (1) as the explosion starts there is a perturbation on the outer surface only, but that surface is stable; (2) the inner surface is unstable, but it has no initial amplitude to grow on; (3) early time feedthrough is minimized because the shell is at its thickest; and finally (4) when feedthrough becomes effective and the inner surface does acquire some perturbations it "goes stable," i.e., the local $Ag<0$. In fact, the close proximity of the stable inner surface has a (small) beneficial effect which inhibits, to some extent, the growth of η_2.

We close this section by considering the oscillation of a shell in such a way that at the end of the cycle the shell returns to its original configuration. We assume that at least one of the interfaces has an initial perturbation of order 1, i.e., the initial conditions read $(\eta_1,\eta_2)_0=(1,0)$ (0,1), or (1,1), but of course not (0,0). The results mentioned below are obtained in a straightforward way by compounding Figs. 7 and 9.

Consider first an implosion followed by an explosion. At the end of the cycle the inner surface perturbation η_1 grows by a factor of 10^{16} in all cases while the outer surface perturbation η_2 grows by 10^9 [10^8 if $\eta_2(0)=0$]. The special initial condition (0,1) has no stabilizing effect here because by the end of the implosion η_1 will have developed a healthy amplitude (about 10^{10}) and the explosion in fact starts with $(\eta_1,\eta_2)=(10^{10},10^3)\approx 10^{10}(1,0)$, and therefore we must use Fig. 9(a) for the explosion phase. From Fig. 9(a) we pick up an additional factor of 10^6 from which we obtain the total factors of 10^{16} and 10^9 quoted above.

If the cycle *starts* with an explosion followed by an implosion,[15] then the special condition (0,1) *does* make a difference to the overall growth factors which are only 10^{11} for η_1 and 10^5 for η_2. Otherwise we obtain the same factors as before: 10^{16} for η_1 and 10^9 for η_2.

Any realistic surface finish will no doubt end up in the nonlinear regime if perturbations grow by such large factors. It is also clear that different implosion or explosion histories, or different density ratios and mode numbers, will yield different growth factors. Admittedly we have considered a very simple implosion and its mirror image explosion (or vice versa). We expect, however, that our results will remain qualitatively correct because they are based primarily on feedthrough of perturbations in shells that thicken up during implosion and thin out during explosion. There is good theoretical support for the mechanism of feedthrough but, unfortunately, no experimental verification so far.

V. A MODEL FOR TURBULENT MIX IN SPHERICAL GEOMETRY

In this section we address the question of turbulent mix in spherical geometry. It is highly probable that multimode perturbations, starting from random initial conditions, grow into the nonlinear regime and interact with each other leading to a "mixing layer" which evolves with time. The most fundamental property of the mixing layer is its width h, and the simplest question is: how does h evolve with time in spherical geometry? The mixing layer has other, perhaps secondary, properties which we do not address in this paper such as scale sizes and their evolution with time, spectrum of turbulent energy, etc. Another question that will be left unanswered is the transition time between the linear and the highly turbulent regime, a question that remains unanswered in plane geometry also.

The evolution of mix at shocked and constantly accelerating interfaces has been observed in plane geometry.[16,17] As far as we know there has been no experimental effort to observe mix in spherical shells due, no doubt, to the extreme difficulty of diagnostics. Here we present a theoretical treatment of the problem. We must warn the reader, however, that unlike the linear stability analysis of Secs. I–IV, where we could start from first principles, the highly nonlinear nature of turbulent mix forbids a first-principles approach and, for that reason, we present only a *model*. Much work, theoretical and experimental, remains to be done.

We consider a two-fluid system as in the $N=2$ case of Sec. III. We assume that the evolution of h is given by Plesset's equation after taking the limit

$$n\to\infty,\quad \eta\to 0,\quad n\eta/R\to c=\text{const}\ . \tag{49}$$

Note that we make no assumptions concerning R. Using Plesset's equation in the form given in Eq. (29), we obtain

$$\frac{1}{R^3}\frac{d}{dt}\left[R^3\frac{dh}{dt}\right]-cA\ddot{R}=0\ , \tag{50}$$

where of course A represents the Atwood number. This equation is the model proposed here.

We should point out that spherical geometry, whose effect on mix we are trying to assess, presents far more difficulties than the above-mentioned nonlinearities which are present in plane geometry also: in spherical geometry the problems are compounded by the presence of a dimensionless variable R/R_0. Scaling or dimensional arguments are often powerful in deducing at least the form of h, but they are no help when it comes to determining dimensionless variables like R/R_0. Furthermore, it is precisely the functional dependence of h on R/R_0 that we are trying to asses, so we cannot neglect it. The planar

limit, $R/R_0 \to 1$, provides only one point of comparison, and does not determine that function. In other words, obtaining the correct planar limit is a necessary condition for any spherical model, but it is not sufficient.

The strength (and perhaps also the weakness) of Eq. (50) is that it is too general. One must specify what kind of $R(t)$ histories can support a mixing width h given by that equation. Unlike Plesset's equation, which cannot be solved in all generality, Eq. (50) can be easily integrated to give $h(t)$ explicitly for any specified $R(t)$:

$$h(t)=h(0)+R_0^3\frac{dh_0}{dt}\int_0^t\frac{dt}{R^3}+cA\int_0^t\left[\frac{1}{R^3}\int_0^t R^3\ddot{R}\,dt'\right]dt\ . \tag{51}$$

For initial conditions we will assume that $h(0)=dh_0/dt=0$, so that only the last term, which is proportional to cA, will survive in the examples considered below. This equation implies, of course, that the evolution of h is independent of initial conditions, which remains to be verified.

For completeness we will present $h(t)$ for all four cases considered in Sec. III, although we are primarily interested in the last two (constant acceleration and a shock). We find

$$h=\frac{cAR_0}{12}\left[1-\frac{R_0}{R}\right]^2\left[2+\frac{3R}{R_0}+\frac{R_0}{R}\right],\quad R=R_0e^{t/T} \tag{52}$$

for case (i);

$$h=2cAR_0\left[1-\frac{R}{R_0}+\ln(R/R_0)\right],\quad R=R_0(1+t/T)^{1/3} \tag{53}$$

for case (ii);

$$h=\frac{cAgt^2}{70}\left[5+16\frac{R_0}{R}+8\left[\frac{R_0}{R}\right]^2+\frac{6}{(R/R_0)-1}\ln(R/R_0)\right],\quad R=R_0+\frac{gt^2}{2} \tag{54}$$

for case (iii); and

$$h=\frac{cA\Delta vt}{2}\left[\frac{R_0}{R}+\left[\frac{R_0}{R}\right]^2\right],\quad \ddot{R}=\Delta v\delta(t),\quad R=R_0+\dot{R}_{0_+}t \tag{55}$$

for case (iv). These equations were obtained by substituting the corresponding $R(t)$ and $\ddot{R}(t)$ in Eq. (51) and carrying out the double integral over time. Only the constant acceleration case was nontrivial. Of course other, perhaps experimental, $R(t)$ histories can always be numerically integrated in Eq. (51). As mentioned above, we are primarily interested in the last two cases, Eqs. (54) and (55).

In the case of a shock let us point out that if the shock *stops* the radial motion, i.e., if $\dot{R}(0_+)=0$ so that $R=R_0$ for $t\geq 0$, then Eq. (55) predicts that the mixing width h will grow linearly in time around such a stationary interface. If this is a "second" shock, one may wish to include the $h(0)$ and dh_0/dt terms of Eq. (51)—they do not spoil the linear-t growth (the slope of h, of course, will be different after a second shock).

We now take the planar limits of our equations, i.e., let $R/R_0 \to 1$. For a constant acceleration Eq. (54) yields

$$h \to \tfrac{1}{2}cAgt^2\ , \tag{56a}$$

which has the correct form gt^2 expected from scaling (such arguments cannot fix the dependence on A, another dimensionless variable). In fact, Eq. (56a) agrees with the experiments of Read and Youngs[17] which can be used to fix the (one) free parameter of the model: $c\approx 0.14$ (h represents the mixing width into the heavier fluid—see Ref. 17). With this value of c we get

$$h=0.07Agt^2\ \text{(plane geometry)}\ . \tag{56b}$$

The planar limit of a shock is even easier to take: from Eq. (55)

$$h\to cA\Delta vt\ . \tag{57a}$$

If c is truly a univeral constant approximately 0.14, then this equation predicts

$$h=0.14A\Delta vt\ \text{(plane geometry)}\ , \tag{57b}$$

a form that we have suggested earlier.[18] The experimental situation on shock-induced mix is not very clear at present (experiments are in progress at several places[19,20]), but a linear dependence on A and on t is not inconsistent with the data available so far. Clearly, it is preferable to have the situation settled first in plane geometry before attempting a spherical shock experiment.

The planar limits given by Eqs. (56) and (57) follow also from the planar limit of the model equation (50) which becomes

$$\frac{d^2h}{dt^2}-cAg=0\ \text{(plane geometry)}\ . \tag{58}$$

No doubt using one "universal constant c to explain and/or predict mix by shocks and constant accelerations in both planar and spherical geometry makes a very tightly constrained model. We expect that a number of effects which we have not taken into account (such as compression) will require the constant c to differ from 0.14. At present we have no theoretical capability to "predict" the value of c. In this paper as in our earlier work we fix it solely on the basis of the experimental work by Read and Youngs[17] on constantly accelerating incompressible fluids. One should limit oneself to positive h or $Ag>0$, although for shocks there is some evidence that the evolution of mix is symmetric between $+A$ and $-A$.

We now define a geometrical factor G by

$$h_{\text{spherical}} = h_{\text{planar}} G \ . \tag{59}$$

From Eqs. (54)–(57) we get

$$G = \left[5 + 16\frac{R_0}{R} + 8\left[\frac{R_0}{R}\right]^2 + \frac{6}{(R/R_0)-1}\ln(R/R_0) \right] \Big/ 35 \tag{60}$$

for a constant acceleration, and

$$G = \frac{R_0}{2R}\left[1 + \frac{R_0}{R}\right] \tag{61}$$

for a shock. We point out that in the very late stages of an explosion ($R/R_0 \to \infty$) Eq. (60) predicts that $G \to \frac{1}{7}$.

In Fig. 10 we plot the above two geometrical factors. Note that the G is larger than 1 for implosions ($G > 1$ for $R/R_0 < 1$) and it is smaller than 1 for explosions ($G < 1$ for $R/R_0 > 1$). In other words, this model predicts that the mixing width for implosions (explosions) will evolve faster (slower) than in plane geometry.

We close this section by repeating our caveats and words of caution. Equation (50) is only a model and not a first-principles result. We cannot estimate the transition time between the linear and the turbulent regime. Equation (50) applies only after that transition has taken place, i.e., in the highly turbulent regime. The fact that it predicts Eq. (56) which agrees with experiments is of course encouraging, but we must remember that we cannot "predict" the constant c—its value, 0.14, is taken from incompressible experiments in plane geometry. Equation (50) also predicts Eq. (57) which, as we mentioned, remains to be verified. Even if it is borne out by experiments, the reader must remember that predicting the "correct" planar limit is only a necessary but by no means sufficient ground for accepting the fully spherical evolution equation (50).

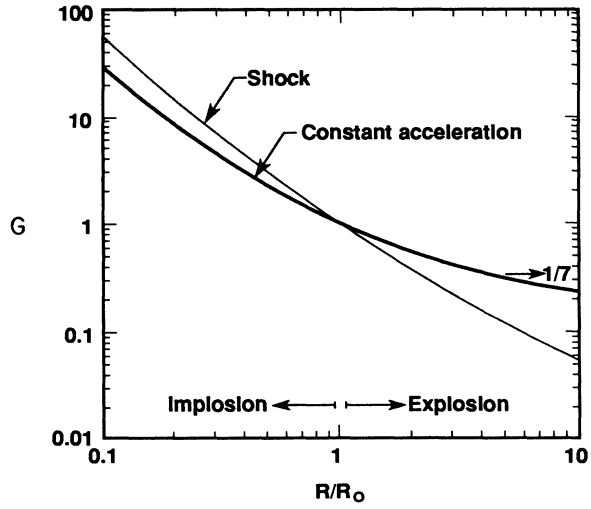

FIG. 10. Geometrical factors for a constant acceleration and a shock. The G's relate spherical and planar mixing widths via $h_{\text{spherical}} = h_{\text{planar}} G$. For the constant acceleration case G asymptotes to $\frac{1}{7}$ as $R/R_0 \to \infty$. For a shock G approaches zero as $R/R_0 \to \infty$ but the mixing width asymptotes to a constant value of $0.07 AR_0$ (see text).

Clearly we need experiments. One would at least like to verify if the geometrical factor is indeed a decreasing function of R/R_0. Explosions may be easier to diagnose, though of course implosions are more important for ICF applications. In either case ingenious methods must be devised to diagnose the mixing layer. The prediction of a finite ($\frac{1}{7}$) geometric effect in explosions even when $R \to \infty$ is interesting ($h \to 0.01 Agt^2$), but it calls for a constant radial acceleration rather than a shock. The geometrical factor for a shock decreases as $R \to \infty$ but note that the mixing width h asymptotes to a limiting value which, from Eq. (55), is

$$h_{\text{shock}} \xrightarrow[R/R_0 \to \infty]{} (c/2) AR_0 \approx 0.07 AR_0 \ . \tag{62}$$

VI. SUMMARY, REMARKS, AND CONCLUSIONS

The main contribution of the present work is to extend Plesset's analysis to include an arbitrary number of incompressible shells. In addition, we found several analytic solutions for $N = 2$ (Plesset's case) and $N = 3$, and proposed a model for turbulent mix in spherical geometry. We also illustrated the evolution of perturbations by numerical examples.

In a system with N fluids there are $N - 1$ interfaces and therefore the phenomenon of interface coupling or feedthrough of perturbations from one interface to another arises for $N \geq 3$. The strength of the coupling is of order $(R_1/R_2)^n$ which reduces to $e^{-k\Delta R}$ in the planar limit ($n \to \infty$, $R_{1,2} \to \infty$, $\Delta R = R_2 - R_1$ finite). Perhaps the most interesting aspect of spherical geometry is the fact that as a shell thickens by convergence or thins out by divergence, i.e., as R_1/R_2 changes, the effectiveness of the interface coupling also changes, as we illustrated by the examples considered in Sec. IV. In contrast, the coupling efficiency remains constant in plane geometry because shell thicknesses do not change with time for incompressible fluids.

The effects of compressibility, which we have neglected in this paper, are expected to be similar as in plane geometry: shells get compressed and hence get thinner as they are subjected to strong pressures as in shocks. Consequently, the effectiveness of feedthrough will increase and the interfaces will be more closely coupled. In addition, the amplitude (for the case of a single scale perturbation) or the mixing width h (for the case of turbulent mix) gets compressed by the passage of a shock. Recently we have carried our 2D numerical simulations[21] on Livermore's compressible hydrocode LASNEX with $N = 2$ and 3. We find that the simulations agree very well with our analytic incompressible results even when a compressible equation of state and large ($\sim 10^{16}$ cm/s^2) accelerations are used as in ICF implosions. The agreement is partly due to the fact that shocks are avoided in constantly accelerating systems. When shocks are present the agreement is poorer and one must take into account the compression of the shell as well as the compression of the

perturbation amplitude. Another Livermore hydrocode (a compressible Lagrangian-Eulerian code) was used to simulate shock tube experiments[22] and in Figs. 11 and 12 we show two examples: the evolution of a single scale perturbation (planar shock impinging on a curved shell, Fig. 11), and the evolution of multiscale perturbations (planar shock impinging on a flat shell with random perturbations, Fig. 12). An analysis of the linear regime indicated[22] that the simple formulas derived following Richtmyer's technique (treat a shock as an instantaneous acceleration) were valid to within 20–30 % if we made allowance for the compressed shell and the compressed amplitude. Of course the highly nonlinear stages shown in Figs. 11 and 12 cannot be described by simple formulas, and the semi-Eulerian code was necessary for such simulations.

In addition to compressibility and nonlinearity a number of other effects (radiation, heat conduction, ablation, etc.) not included in our analytic theory require numerical simulations for a realistic treatment of ICF capsule implosions. A model combining theory and simulation has been proposed by Haan.[23] The effects listed above

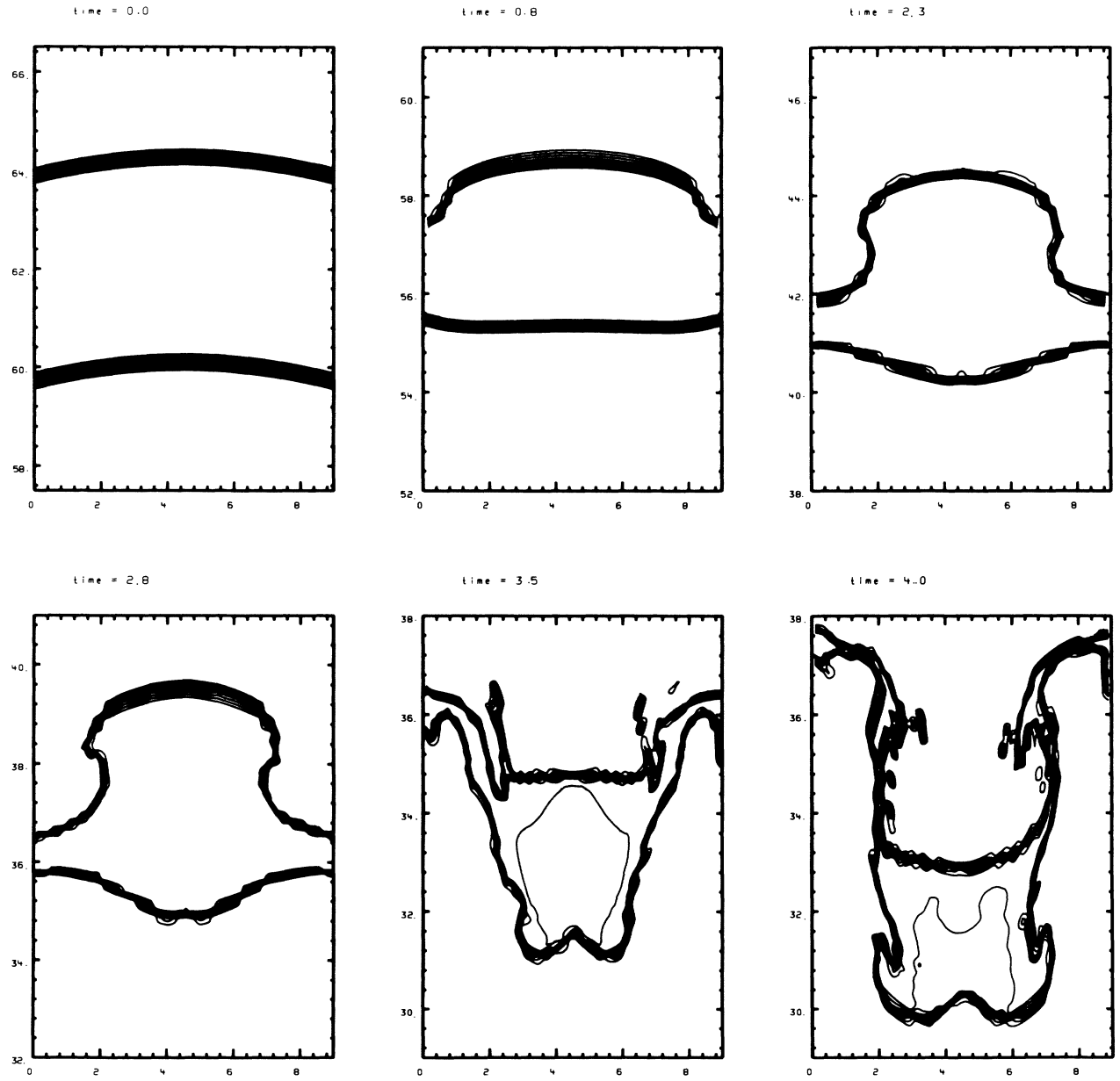

FIG. 11. Isodensity contours in a shock tube simulation in which a plane shock of Mach number 1.2 passes from air into a curved Freon shell 4 cm thick and, after reflecting from a wall 60 cm away, reshocks the Freon shell at $t \approx 3.0$ ms. The direction of the first (second) shock is vertically down (up). Distances are in centimeters and times in milleseconds. For details see Ref. 22.

are taken into account by direct numerical simulations in the linear regime and the nonlinear effects in the presence of multiscale perturbations are assumed to begin when $n^2\eta(t,n,m)\sim vR(t)$, with v a constant number between 3 and 5 [note that this differs from our linearity condition for single scale given in Eq. (7)]. We have carried out LASNEX simulations of single scale perturbations in *laser-driven targets* and we find that linear growth rates are 40–80 % of classical.[21] Radiation effects are found to be important only at high laser intensities ($\geq 10^{15}$ W/cm^2). We have also carried out a few multiscale perturbations and we find that the appearance of new modes is consistent with the weakly nonlinear classical theory, provided that ablative stabilization is taken into account. Fully 3D turbulent calculations with ablation have also been reported.[24]

The theoretical results presented in this paper help our understanding of feedthrough and its time dependence because of spherical geometry in ICF implosions. Our analytic solutions can also serve as tests for 2D and 3D codes. Until 3D spherical capsule implosions are realistically simulated including the various effects listed above, we will have pieces of theoretical analysis on the one hand and pieces of code simulation on the other, and the

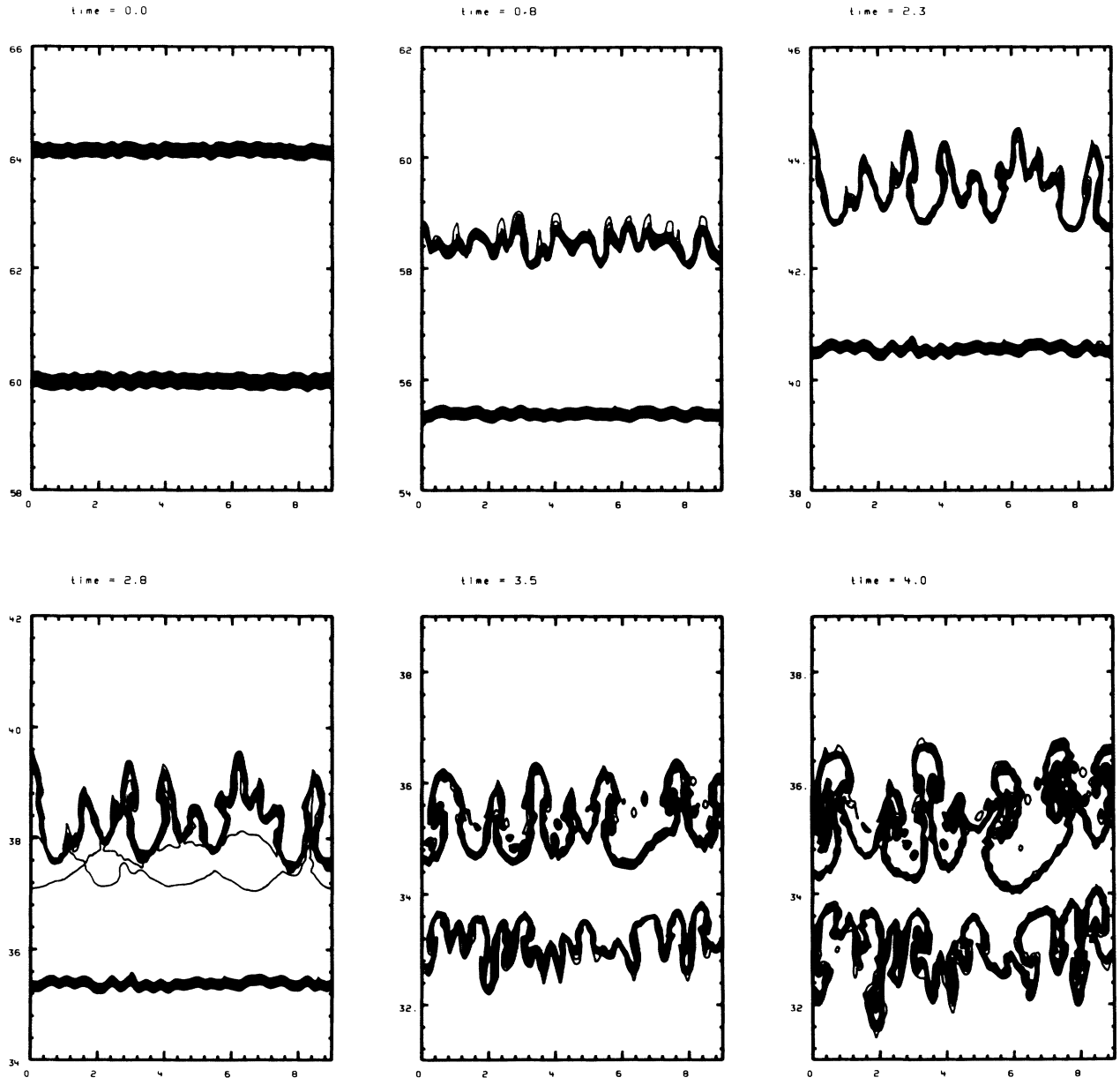

FIG. 12. Same as Fig. 11 with a plane Freon shell having random initial perturbations (maximum peak-to-valley amplitude=0.1 cm) at both surfaces. Doubling the initial amplitude to 0.2 cm had only a small effect on the late time (t =4.0 ms) appearance of the shell.

two must be judiciously combined to make reliable predictions on how the yield of ICF capsules may be degraded because of mix. A definite prediction of the model presented in Sec. V is that, while single scale perturbations clearly depend on initial conditions such as amplitude and wavelength, multiscale perturbations in the highly nonlinear regime develop a mixing width that is largely independent of initial conditions. This is verified by planar experiments with constant acceleration,[17] but the pertinent information in the presence of shocks or spherical geometry is not available.

On the experimental side spherical systems are much more difficult to diagnose than planar ones. Cylinders stand midway in difficulty between the two and some experimental results have been reported,[25] and we hope to investigate multishell cylindrical systems and their stability in the future. We expect that most, if not all, of the convergence effects found in spherical geometry will be captured by cylindrical systems also.

Finally, we hope future experiments will detect some of the phenomena (feedthrough, freeze-out, critical modes, etc.) discussed here. We believe they are of interest in and of themselves. Similarly, we hope that our definition of the geometrical factor relating $h_{\text{spherical}}$ to h_{planar} will be of some use to experimentalists. Clearly, our predictions for single scale perturbations and for turbulent mix must be tested in simple laboratory experiments before one augments them with the effects discussed above and applies them to astrophysical or ICF systems.

ACKNOWLEDGMENTS

This research was supported by the U.S. Department of Energy under Contract No. W-7405-ENG-48.

APPENDIX

In this appendix we give the details of the four class-B analytic solutions mentioned in Sec. III. The class-A solutions reported there are straightforward to obtain.

(i) $R=R_0e^{t/T}$, where T represents a time constant. Throughout this paper a positive time constant will be associated with explosions and a negative time constant will be associated with implosions. Note that $\ddot{R}/R=1/T^2$ hence $\ddot{R}>0$ whether $T>0$ (explosion) or $T<0$ (implosion).

With $R=R_0e^{t/T}$ Eq. (27) reduces to

$$\frac{d^2\eta}{dt^2}+\frac{3}{T}\frac{d\eta}{dt}-nA(n)\frac{1}{T^2}\eta=0\ , \tag{A1}$$

whose solution is

$$\eta(t)=\eta_0\frac{\gamma_+e^{\gamma_-t}-\gamma_-e^{\gamma_+t}}{\gamma_+-\gamma_-}+\dot{\eta}_0\frac{e^{\gamma_+t}-e^{\gamma_-t}}{\gamma_+-\gamma_-}\ , \tag{A2}$$

where

$$\gamma_\pm=\frac{1}{2T}[-3\pm\sqrt{9+4nA(n)}]\ . \tag{A3}$$

One may take advantage of the radial motion, $R=R_0e^{t/T}$, to write the exponential functions in terms of R:

$$e^{\gamma_\pm t}=(R/R_0)^{\gamma_\pm T}=(R/R_0)^{[-3\pm\sqrt{9+4nA(n)}]/2}\ . \tag{A4}$$

We see that for the case $R=R_0e^{t/T}$ where we have an exponential implosion or explosion the perturbation amplitude $\eta(t)$ evolves exponentially in time. This should be contrasted with plane geometry where a *constant acceleration* leads to an exponentially growing amplitude.

The solution given above is valid for arbitrary $nA(n)$. To compare with the doubly restricted cases, we first let $nA(n)=-2$. Then $\gamma_+=-1/T$, $\gamma_-=-2/T$, and Eq. (A2) becomes

$$\begin{aligned}\eta&=\eta_0(2e^{-t/T}-e^{-2t/T})+\dot{\eta}_0T(e^{-t/T}-e^{-2t/T})\\&=(2\eta_0+\dot{\eta}_0T)(R_0/R)-(\eta_0+\dot{\eta}_0T)(R_0/R)^2\ ,\end{aligned} \tag{A5}$$

which agrees with the corresponding class-A solution when we let $R=R_0e^{t/T}$ in Eq. (30).

If we let $nA(n)=0$ (critical modes) then $\gamma_+=0$ and $\gamma_-=-3/T$, so that Eq. (A2) now becomes

$$\begin{aligned}\eta(t)&=\eta_0+\frac{\dot{\eta}_0T}{3}(1-e^{-3t/T})\\&=\eta_0+\frac{\dot{\eta}_0T}{3}[1-(R_0/R)^3]\ ,\end{aligned} \tag{A6}$$

which agrees with the corresponding solution when we set $R=R_0e^{t/T}$ in Eq. (31). Equation (A6) exhibits the expected critical behavior, i.e., $\eta(t)=\eta_0$ if $\dot{\eta}_0=0$.

(ii) $R=R_0(1+t/T)^{1/3}$. Note that $\ddot{R}=-2R_0^6/9T^2R^5$ and therefore $\ddot{R}<0$ whether $T>0$ (explosion) or $T<0$ (implosion).

Plesset's equation for this case can be solved by making a change of variables: define

$$x=\ln\left[1+\frac{t}{T}\right]=3\ln(R/R_0) \tag{A7}$$

so that $d/dt=(e^{-x}/T)d/dx$. Equation (29) reduces to

$$\frac{d^2\eta}{dx^2}+\frac{2}{9}nA(n)\eta=0\ , \tag{A8}$$

whose solution is

$$\eta(x)=\eta(0)\cos(\gamma x)+\frac{\eta_x(0)}{\gamma}\sin(\gamma x)\ , \tag{A9}$$

with $\gamma=\frac{1}{3}\sqrt{2nA(n)}$.

In this equation $\eta_x(0)=(d\eta/dx)_{x=0}=T\dot{\eta}_0$. When described in terms of x, the evolution of η is extremely simple: if $nA(n)>0$, then γ is real and η oscillates with x; if $nA(n)<0$, then γ is imaginary and therefore η grows exponentially with x.

Writing Eq. (A9) in terms of the "real" variable R/R_0, we find

$$\eta(t)=\frac{\eta_0}{2}\left[\left[\frac{R}{R_0}\right]^{i\sqrt{2nA(n)}}+\left[\frac{R}{R_0}\right]^{-i\sqrt{2nA(n)}}\right]+\frac{3\dot{\eta}_0 T}{2i\sqrt{2nA(n)}}\left[\left[\frac{R}{R_0}\right]^{i\sqrt{2nA(n)}}-\left[\frac{R}{R_0}\right]^{-i\sqrt{2nA(n)}}\right] . \quad \text{(A10)}$$

This form is useful for checking against the class-A solutions. If we let $nA(n)=-2$, we get

$$\eta(t)=\frac{\eta_0}{2}\left[\left[\frac{R}{R_0}\right]^{2}+\left[\frac{R}{R_0}\right]^{-2}\right]+\frac{3\dot{\eta}_0 T}{4}\left[\left[\frac{R}{R_0}\right]^{2}-\left[\frac{R}{R_0}\right]^{-2}\right] , \quad \text{(A11)}$$

which agrees with the result obtained from Eq. (30) after substituting $R=R_0(1+t/T)^{1/3}$ in that equation. This is a nontrivial check. Note that in this case $\eta(t)$ will grow quadratically with R whether the system implodes ($R/R_0<1$) or explodes ($R/R_0>1$), though in principle it is possible to cancel the growing term with a suitable choice of $\dot{\eta}_0$.

For critical modes [$nA(n)=0$] Eq. (A10) becomes

$$\eta(t)=\eta_0+3\dot{\eta}_0 T\ln(R/R_0)=\eta_0+\dot{\eta}_0 T\ln(1+t/T) , \quad \text{(A12)}$$

which agrees with Eq. (31) when we substitute $R=R_0(1+t/T)^{1/3}$ in that equation.

(iii) $R(t)=R_0+\dot{R}_0 t+\frac{1}{2}gt^2$, $g=$const. This constant acceleration case turns out to be the most complicated case considered in this paper. To solve Plesset's equation we again make a change of variables:

$$x=\frac{1}{2\alpha}\left[t+\frac{\dot{R}_0}{g}+\alpha\right], \quad \alpha^2=\frac{\dot{R}_0^2}{g^2}-\frac{2R_0}{g} , \quad \text{(A13)}$$

so that

$$R=2\alpha^2 gx(x-1), \quad \dot{R}=2(x-\tfrac{1}{2})\alpha g, \quad \ddot{R}=g . \quad \text{(A14)}$$

Plesset's equation becomes

$$x(1-x)\frac{d^2\eta}{dx^2}+6(\tfrac{1}{2}-x)\frac{d\eta}{dx}+2nA(n)\eta=0 , \quad \text{(A15)}$$

whose solution is the hypergeometric function[26] $F(a,b;c;x)$ where

$$a=\frac{5+\sqrt{25+8nA(n)}}{2} , \quad b=\frac{5-\sqrt{25+8nA(n)}}{2} , \quad \text{(A16)}$$

and

$$c=3 .$$

It is ironic that the constant acceleration case, probably assumed to be the simplest by Binnie[9] and by Gupta and Lawande,[6,11] turns out to be quite a complicated one. The constants a and b given above were derived by comparing Eq. (A15) with the differential equation obeyed by the hypergeometric function in the notation of Ref. 26. They satisfy $ab=-2nA(n)$ and $a+b+1=6$.

A numerical example with a constant acceleration and deceleration was given in Sec. III B. Rather than consult tables we solve Plesset's equation numerically. This approach has the obvious advantage that in this way one can evolve $\eta(t)$ for any implosion or explosion history in the subroutine calling for $R(t)$. We used the analytical solutions found in cases (i) and (ii) as a check of our numerical integration technique.

The special case $\ddot{R}=g=0$ can be trivially integrated because Eq. (29) implies that $R^3\dot{\eta}=$const. This case is formally similar to case (ii) in class A, but note that here we make *no* simplifying assumptions concerning $nA(n)$. The solution is still given by Eq. (31) after setting

$$R(t)=R_0+\dot{R}_0 t=R_0(1+t/T) \quad (g=0) \quad \text{(A17)}$$

so that

$$\eta(t)=\eta_0+\frac{\dot{\eta}_0 T}{2}[1-(R_0/R)^2] \quad \text{(A18a)}$$

$$=\eta_0+\dot{\eta}_0 t\frac{1+t/2T}{(1+t/T)^2} . \quad \text{(A18b)}$$

(iv) $\ddot{R}=\Delta v\,\delta(t-t_s)$. We refer to this case as a "shock," i.e., an instantaneous acceleration occurring at $t=t_s$ in which the radial velocity is changed from $\dot{R}(t_{s_-})$ to $\dot{R}(t_{s_+})$ but of course the position R is not changed instantaneously. We have defined $\Delta v=\dot{R}(t_{s_+})-\dot{R}(t_{s_-})$. As we discussed in Sec. II, the perturbation amplitudes also behave in a similar manner: their values are not changed instantaneously but they do acquire a new growth rate. Integrating Plesset's equation over $t_{s_-}<t<t_{s_+}$, where the subscripts $\pm$ refer to times immediately before and after the shock which is assumed to arrive at $t=t_s$, we get

$$\dot{\eta}(t_{s_+})=\dot{\eta}(t_{s_-})+nA(n)\frac{\Delta v}{R_s}\eta(t_s) . \quad \text{(A19)}$$

This result is of course similar to the planar case [see Eq. (10)]. R_s is the radius at shock arrival time. Note that critical modes $nA(n)=0$ are not affected by a shock.

Let us consider a shock at $t=0$ followed by a constant velocity. Since postshock $g=0$, the evolution is given by Eq. (A18) with the shock setting the "initial" conditions, i.e.,

$$\eta_0\rightarrow\eta_0 ,$$

$$\dot{\eta}_0\rightarrow\dot{\eta}(0_+)=\dot{\eta}(0_-)+nA(n)\frac{\Delta v}{R_0}\eta_0 .$$

Substituting these expressions into Eq. (A18a) we get

$$\eta(t)=\eta_0+\frac{T}{2}\left[\dot{\eta}(0_-)+nA(n)\frac{\Delta v}{R_0}\eta_0\right]\left[1-\left[\frac{R_0}{R}\right]^2\right] , \quad \text{(A20)}$$

where $\Delta v=\dot{R}(0_+)-\dot{R}(0_-)$ and $T=R_0/\dot{R}(0_+)$. If there was truly no motion before this $t=0$ shock, i.e., if $\dot{\eta}(0_-)=\dot{R}(0_-)=0$, then $\Delta v=\dot{R}(0_+)=R_0/T$ and Eq. (A20) simplifies to

$$\eta(t)=\eta_0\left\{1+\frac{nA(n)}{2}\left[1-\left[\frac{R_0}{R}\right]^2\right]\right\} \tag{A21}$$

as reported in Eq. (34).

We now consider the reverse case: constant velocity *followed* by a shock at $t=t_s$. The perturbation evolves according to Eq. (A18) until $t=t_s$, when the shock arrives and changes the velocity $\dot{R}(t_{s_-})$ to $\dot{R}(t_{s_+})$ and $\dot{\eta}(t_{s_-})$ to $\dot{\eta}(t_{s_+})$. We will define $\dot{R}(t_{s_-})=R_0/T_-$ and $\dot{R}(t_{s_+})=R_s/T_+$. The shock may stop the radial motion of the interface, i.e., $\dot{R}(t_{s_+})=0$, which will be a limiting case $T_+\to\infty$. We can obtain $\dot{\eta}(t_{s_-})$ by differentiating Eq. (A18b); a faster way is to note that $R^3\dot{\eta}$ is conserved when the interface moves with constant velocity and therefore

$$\dot{\eta}(t_{s_-})=\frac{R_0^3}{R_s^3}\dot{\eta}_0 .$$

Substituting this value in Eq. (A19) we get

$$\dot{\eta}(t_{s_+})=\frac{R_0^3}{R_s^3}\dot{\eta}_0+nA(n)\frac{R_s/T_+-R_0/T_-}{R_s}\eta(t_s) \tag{A22}$$

where, from Eq. (A18),

$$\eta(t_s)=\eta_0+\dot{\eta}_0\frac{T_-}{2}[1-(R_0/R_s)^2] . \tag{A23}$$

As we mentioned above, the shock may stop the radial motion of the interface. The evolution of perturbations at a "stationary" interface is in fact the simplest of all: setting $\ddot{R}=\dot{R}=0$ in Plesset's equation it reads $d^2\eta/dt^2=0$ and therefore

$$\eta(t)=\eta(0)+\dot{\eta}(0)t . \tag{A24}$$

If the stopping is done with the help of a shock at $t=t_s$, we simply translate Eq. (A24) in time to read

$$\eta(t>t_s)=\eta(t_s)+\dot{\eta}(t_{s_+})(t-t_s) . \tag{A25}$$

No matter how the stopping is done, perturbations grow linearly with time on a stationary interface.

Instead of, or in addition to, stopping the radial motion of an interface a shock may, if properly timed, stop the motion of the perturbations themselves by setting $\dot{\eta}(t_{s_+})=0$. This is the "freeze-out" phenomenon which we reported earlier for the planar case.[5] It is clear from Eq. (A19) that one can arrange to have $\dot{\eta}(t_{s_+})=0$ by canceling $\dot{\eta}(t_{s_-})$ immediately before the shock against the $\dot{\eta}$ induced by the shock, i.e., against $nA(n)(\Delta v/R_s)\eta(t_s)$.

The shock timing necessary to freeze out an amplitude is obtained by setting to zero the lhs of Eq. (A22) after substituting Eq. (A23) for $\eta(t_s)$. To compare with the planar result we write down one of the intermediate steps in the algebra:

$$\dot{\eta}_0+(R_s/R_0)^2\frac{nA(n)}{R_0}\left[\frac{R_s}{T_+}-\frac{R_0}{T_-}\right]\eta_0 = -\frac{nA(n)}{R_0}\left[\frac{R_s}{T_+}-\frac{R_0}{T_-}\right]\frac{\dot{\eta}_0}{2}t_s\left[\frac{R_s}{R_0}+1\right] . \tag{A26}$$

If we now let $n\to kR$ with finite k but $R\to\infty$, hence $n\to\infty$, then $A(n)\to A$, $R_s/R_0\to 1$, $R_s/T_+-R_0/T_-=v(t_{s_+})-v(t_{s_-})=\Delta v$, and Eq. (A26) reduces to

$$\dot{\eta}_0+kA\Delta v\eta_0=-kA\Delta v\dot{\eta}_0 t_s , \tag{A27}$$

which agrees with the planar result [Eq. (10) of Ref. 5].

The final result for spherical geometry is

$$\left[\frac{R_s}{R_0}\right]^2=\left[1+\frac{t_s}{T_-}\right]^2=\frac{\dot{\eta}_0\{[nA(n)/2][(R_s/R_0)(T_-/T_+)-1]-1\}}{nA(n)[(R_s/R_0)(T_-/T_+)-1](\dot{\eta}_0/2+\eta_0/T_-)} , \tag{A28}$$

which determines R_s (or t_s) necessary for freeze-out.

The very special case where the "second" shock stops R *and* freezes η can be obtained from Eq. (A28) by taking the limit $T_+\to\infty$:

$$\left[\frac{R_s}{R_0}\right]^2=\left[1+\frac{t_s}{T_-}\right]^2=\frac{\dot{\eta}_0[2+nA(n)]}{nA(n)(\dot{\eta}_0+2\eta_0/T_-)} . \tag{A29}$$

So far we have kept the initial conditions η_0 and $\dot{\eta}_0$ arbitrary. If they actually are set by a "first" shock, then the two are related:

$$\dot{\eta}_0=nA(n)\frac{\eta_0}{T_-} , \tag{A30}$$

and we find that η_0 drops out of the freeze-out condition: Eq. (A28) becomes

$$\left[\frac{R_s}{R_0}\right]^2=\left[1+\frac{t_s}{T_-}\right]^2 =\frac{[nA(n)/2][(R_s/R_0)(T_-/T_+)-1]-1}{[(R_s/R_0)(T_-/T_+)-1][1+nA(n)/2]} . \tag{A31}$$

For example, if $nA(n)=10$ and the velocity ratio is 2 (or $\frac{1}{2}$) we get $(R_s/R_0)^2=\frac{2}{3}$ (or $\frac{7}{6}$). There are many possibilities, especially if we remember that the shocks may be

directed inwards or outwards, i.e., either T_+ or T_- or both may be positive or negative.

Note that *it is not possible* to stop R *and* freeze η if the initial conditions are set by a first shock: substituting Eq. (A30) into Eq. (A29) we get $R_s = R_0$, i.e., $t_s = 0$. When we consider that there are three possible events: (1) setting initial conditions by a shock, (2) second shock stopping the radial motion, and (3) second shock stopping the perturbations (freeze-out), we conclude that one can choose any single event or any combination of two events, but not all three.

The situation is the same in plane geometry. If the initial conditions are set by a first shock, then $\dot{\eta}_0 = kAv_i\eta_0$ and Eq. (A27) reduces to

$$t_s = -\frac{v_f/v_i}{\Delta v k A}\ , \tag{A32}$$

again independent of the initial amplitude η_0. This is the shock timing required to freeze-out an amplitude with initial conditions set by a shock. It is clear that we cannot add a third requirement of stopping the radial motion ($v_f = 0$). Again, any single or two out of the three events mentioned in the preceding paragraph can be selected, but not all three.

[1]Lord Rayleigh, *Scientific Papers* (Dover, New York, 1965), Vol. 2; G. I. Taylor, Proc. R. Soc. London, Ser. A **201**, 192 (1950).

[2]R. D. Richtmyer, Commun. Pure Appl. Math. **13**, 297 (1960); E. E. Meshkov, Izv. Akad. Nauk SSSR, Mekh. Zhidk. Gaza **5**, 151 (1969).

[3]For a review see D. H. Sharp, Physica D **12**, 3 (1984).

[4]K. O. Mikaelian, Phys. Rev. Lett. **48**, 1365 (1982); Phys. Rev. A **26**, 2140 (1982); **28**, 1637 (1983).

[5]K. O. Mikaelian, Phys. Rev. A **31**, 410 (1985).

[6]N. K. Gupta and S. V. Lawande, Plasma Phys. Contr. Fusion **28**, 925 (1986).

[7]R. Bellman, *Stability of Differential Equations* (McGraw-Hill, New York, 1953); G. I. Bell, Los Alamos National Laboratory Report No. LA-1321, 1951 (unpublished). For historical remarks see G. Birkhoff (Ref. 8).

[8]G. Birkhoff, Quart. Appl. Math. **12**, 306 (1954); **13**, 451 (1956).

[9]A. M. Binnie, Proc. Cambridge Philos. Soc. **49**, 151 (1953).

[10]M. S. Plesset, J. Appl. Phys. **25**, 96 (1954).

[11]N. K. Gupta and S. V. Lawande, Phys. Rev. A **33**, 2813 (1986).

[12]K. O. Mikaelian, Phys. Rev. A **36**, 411 (1987).

[13]M. S. Plesset and T. P. Mitchell, Quart. Appl. Math. **13**, 419 (1956).

[14]This is similar to the planar geometry treatment: in the first (last) fluid the velocity eigenfunction is e^{ky} (e^{-ky}), but in the intermediate layers it is a linear combination of $e^{\pm ky}$ (see Ref. 4).

[15]There are few physical examples: a star may oscillate in time, or an unsuccessful supernova explosion may implode back on itself.

[16]V. A. Andronov *et al.*, Zh. Eksp. Teor. Fiz. **71**, 806 (1976) [Sov. Phys.—JETP **44**, 424 (1976)]; S. G. Zaitsev *et al.*, Dokl. Akad. Nauk SSSR **283**, 94 (1985) [Sov. Phys.—Dokl. **30**, 579 (1985)].

[17]K. I. Read, Physica D **12**, 45 (1984); K. I. Read and D. L. Youngs, United Kingdom Atomic Weapons Research Establishment Report No. O11/83, 1983 (unpublished).

[18]K. O. Mikaelian, Physica D **36**, 343 (1989).

[19]*Proceedings of the Princeton Workshop on the Physics of Compressible Turbulent Mixing,* Springer Verlag Series Lecture Notes in Engineering, Princeton, 1988, edited by W. T. Dannevik, A. C. Buckingham, and C. E. Leith (Springer-Verlag, Berlin, in press), Vols. I and II.

[20]B. Sturtevant, in *Shock Waves and Shock Tubes,* Proceedings of the 16th International Symposium on Shock Waves and Shock Tubes, Aachen, 1987, edited by H. Gronig (VCH , New York, 1988), p. 89. See also Ref. 19.

[21]K. O. Mikaelian, Phys. Rev. A (to be published).

[22]K. O. Mikaelian, Report No. UCID-21328, Lawrence Livermore National Laboratory (1988) (unpublished); in Ref. 19.

[23]S. W. Haan, Phys. Rev. A **39**, 5812 (1989).

[24]J. P. Dahlburg, J. H. Gardner, and G. D. Doolen, Bull. Am. Phys. Soc. **34**, 2114 (1989), Abstract No. 7E10.

[25]Experimental results in cylindrical geometry have been reported by V. A. Andronov *et al.*, Dokl. Akad. Nauk SSSR **264**, 76 (1982) [Sov. Phys.—Dokl. **27**, 393 (1982)]; and N. Wilke *et al.* (unpublished).

[26]E. T. Whittaker and G. N. Watson, *Modern Analysis* (Cambridge University Press, London, 1963), Chap. XIV.